



Changing effects of external forcing on Atlantic-Pacific interactions

Soufiane Karmouche^{1,2}, Evgenia Galytska^{1,2}, Gerald A. Meehl³, Jakob Runge^{4,5}, Katja Weigel^{1,2}, and Veronika Eyring^{2,1}

¹University of Bremen, Institute of Environmental Physics (IUP), Bremen, Germany

²Deutsches Zentrum für Luft- und Raumfahrt e.V. (DLR), Institut für Physik der Atmosphäre, Oberpfaffenhofen, Germany

³Climate and Global Dynamics Laboratory, National Center for Atmospheric Research (NCAR), Boulder, CO, USA

⁴Deutsches Zentrum für Luft- und Raumfahrt e.V. (DLR), Institut für Datenwissenschaften, Jena, Germany

⁵Fachgebiet Klimainformatik, Technische Universität Berlin, Berlin, Germany

Correspondence: Soufiane Karmouche (sou_kar@uni-bremen.de)

Abstract. Recent studies have highlighted the increasingly dominant role of external forcing in driving Atlantic and Pacific Ocean variability during the second half of the 20th century. This paper provides insights into the underlying mechanisms driving interactions between modes of variability over the two basins. We define a set of possible drivers of these interactions and apply causal discovery to reanalysis data, an ensemble of pacemaker simulations where the observed El Niño Southern Oscillation (ENSO) is prescribed, and a pre-industrial control simulation. We also utilize large ensemble means of historical simulations from the Coupled Model Intercomparison Project Phase 6 (CMIP6) to quantify the effect of external forcing and improve the understanding of its impact. By conducting a causal analysis of the historical time series, a regime switch is identified in the interactions between major modes of Atlantic and Pacific climate variability. Causal networks derived from pacemaker simulations support this finding and further demonstrate that the effect of external forcing could favor an Atlantic-driven regime between 1985 and 2014 where warming tropical North Atlantic sea surface temperatures induce a La Niña-like cooling in the equatorial Pacific during the following season through a strengthening of the Pacific Walker Circulation. This negative sign effect was not detected when the historical external forcing signal is removed in the pacemaker ensemble. The analysis of the pre-industrial control run further supports the notion that the Atlantic and Pacific modes of natural climate variability exert contrasting impacts on each other even in the absence of external forcing. We show that causal discovery can quantify previously unknown connections and thus provides important potential to contribute to a deeper understanding of the mechanisms driving changes in regional and global climate variability.

1 Introduction

One of the biggest challenges in climate science is associated with disentangling the effects of internal climate variability and external forcings and robust quantification of their impacts. External forcing includes changes to the climate system caused by natural factors such as volcanic eruptions, solar radiation, or from the human emission of greenhouse gas (GHG) and aerosols. Internal climate variability, on the other hand, refers to the inherent fluctuations in the climate system that arise from complex interactions between the atmosphere, oceans, land, and cryosphere (Cassou et al., 2021). For instance, the interactions between the ocean and atmosphere produce unique patterns of variability at different time scales, such as El Niño-



Southern Oscillation (ENSO, Bjerknes, 1966, 1969; Neelin et al., 1998), Pacific Decadal Variability (PDV, Mantua et al., 1997; Newman et al., 2016), and Atlantic Multidecadal Variability (AMV, Trenberth and Shea, 2006; Zhang et al., 2019). Despite the considerable advancements through different phases of the Coupled Model Intercomparison Project (CMIP), including the ability to represent the statistical properties and spatial patterns of modes of climate variability, accurately simulating them as in the observed record still poses daunting challenges (Eyring et al., 2019; Fasullo et al., 2020; Karmouche et al., 2023). In addition to the short historical record, the intricate nature of the climate system and the non-linear characteristics of natural climate variability impose inherent limitations on predictability and introduce inseparable uncertainty into climate model projections (Deser et al., 2012; Meehl et al., 2013; Fasullo et al., 2020; Eyring et al., 2021; Deser and Phillips, 2023). This underlines the importance of studying natural climate variability modes and their teleconnections to advance our understanding of the climate system and improve the reliability of climate model projections (Deser and Phillips, 2023).

Previous studies have explored connections between the Atlantic and Pacific basins, focusing on the influence of the Walker circulation on both interannual and decadal timescales (Latif and Grötzner, 2000; McGregor et al., 2014; Meehl et al., 2016; Ruprich-Robert et al., 2017; Meehl et al., 2021). Other studies found that the Atlantic drives the Pacific, while the Pacific can also drive the Atlantic, and there are influences between the two through the tropical Indian Ocean (Kumar et al., 2014; Li et al., 2016; Ruprich-Robert et al., 2017; Levine et al., 2017; Meehl et al., 2016; Yang et al., 2020). For example, on the decadal timescale, Meehl et al. (2021) demonstrate how a positive AMV can lead to a negative PDV through anomalous Walker circulation. They showed that a negative PDV, which triggers a same-sign response in the Atlantic, contributes to AMV's transition from a positive to a negative phase (Fig. 3 in Meehl et al., 2021). The study highlights that in addition to the tropical Walker circulation (Bjerknes, 1969), positive convective heating and precipitation anomalies in the tropical Pacific can establish connections to extra-tropical modes of atmospheric variability, e.g. the Pacific-North American pattern (PNA), which also contribute to the same-sign effect of the Pacific on the Atlantic. The tropical pathway connecting the Pacific and the Atlantic happens mainly through modifications to the Walker circulation affecting large-scale tropical weather systems. On the other hand, the extratropical northern hemisphere teleconnections illustrated through the PNA and North Atlantic Oscillation (NAO, Barnett, 1985; Brönnimann et al., 2007; Scaife and et al., 2014), not only connect the Atlantic-Pacific basins but also play important roles in modulating Arctic sea ices responses (Polyakov and Johnson, 2000; Meehl et al., 2018; Galytska et al., 2022) and shaping European climate (Brönnimann et al., 2007; Brönnimann, 2007). On the seasonal and interannual timescales, a study by Park et al. (2023) on inter-basin interactions between the Atlantic and Pacific Oceans showed that ENSO affects sea surface temperature anomalies (SSTAs) of the Tropical North Atlantic (TNA) during the spring and summer through tropical and extratropical pathways (also discussed in Meehl et al., 2016, 2021). Conversely, SST variability of TNA can also influence an ENSO event during the following boreal winter by modifying anomalous low-level zonal winds through atmospheric teleconnections over the equatorial western Pacific (Park and Li, 2019; Park et al., 2023). The high SSTAs in the tropical Atlantic trigger an atmospheric response that strengthens the connection between TNA and ENSO (Wang et al., 2017b; Park et al., 2019). The impact of the TNA on ENSO, which has become more significant since the mid-1980s is associated with an increase in the climatological mean SST in the tropical Atlantic, which can be attributed to a positive phase shift of AMV and/or human-caused warming (Park and Li, 2019; Meehl et al., 2021; Park et al., 2023). In turn, the effect of ENSO



on TNA has decreased since the mid-1980s, supporting the existence of two regimes of contrasting responses as proposed
60 by (Meehl et al., 2021) and described by Park et al. (2023) as a Pacific-driven regime (1950 to mid-1980s) as opposed to an
Atlantic-driven regime (from mid-1980s to 2014), where both span over multiple decades.

While the debate over the precise attribution of recent warming trends and the mid-1980s regime switch is still ongoing,
it is evident that signals from natural internal variability, GHG-induced warming, and aerosol-cooling all play roles in the
observed changes in global temperature variability over the historical record (Brönnimann, 2007; Meehl et al., 2013; Kosaka
65 and Xie, 2013; Dong et al., 2014; Mann et al., 2014; McGregor et al., 2014; Li et al., 2016; Meehl et al., 2016; Kucharski
et al., 2016; Smith et al., 2016; Dong and McPhaden, 2017; Hausteine et al., 2019). There is growing evidence, however, that
in the Atlantic, external forcing is responsible for the recent AMV changes and its widespread impacts (Murphy et al., 2017;
Klavans et al., 2022; He et al., 2023). In addition to that, differences in the considered timescales and limited coverage of the
in-situ observations over the tropical Pacific contribute to a lack of consensus between previous studies on the reasons behind
70 the recently observed 1979-2014 strengthening of the Walker circulation (Vecchi and Soden, 2007; Power and Kociuba, 2011;
L'Heureux et al., 2013; DiNezio et al., 2013; Kociuba and Power, 2015). Findings from Chung et al. (2019) indicate that
internal variability linked to the Interdecadal Pacific Oscillation (IPO, similar to PDV) likely played the dominant role in the
recent strengthening of the Walker circulation. Other studies, however, emphasize the role of SST variability in neighboring
ocean basins, such as the Atlantic (Kucharski et al., 2011; McGregor et al., 2014) and/or the Indian Ocean (Luo et al., 2012), in
75 modulating the tropical Pacific variability. This means that the anthropogenic contribution to the Atlantic SST warming during
the recent decades (Watanabe and Tatebe, 2019; Klavans et al., 2022) might have influenced the Pacific variability and its effect
on the recent strengthening of the Walker circulation.

To address the effects of a changing climate on the interactions between these modes, it is necessary to isolate internal
variability from external forcing. While the “signal-to-noise paradox” in climate models is still a topic of debate (Scaife and
80 et al., 2014; Wang et al., 2017a; Sato et al., 2018; Smith et al., 2019; Chylek et al., 2020; Klavans et al., 2021, 2022), the
use of large ensemble simulations has been proven to be extremely helpful to capture the observed trends and to help the
detection and attribution of anthropogenic climate change in the observational record (Meehl et al., 2013; Menary et al., 2020;
Borchert et al., 2021; Deser, 2020; Tebaldi et al., 2021; Klavans et al., 2022; Deser and Phillips, 2023). Studies proved that
large ensembles can provide a robust sampling of models’ internal variability and help assess externally forced changes in the
85 characteristics of simulated internal variability (Menary et al., 2020; Borchert et al., 2021; Klavans et al., 2022; Deser and
Phillips, 2023). Therefore, this paper utilizes large ensembles from CMIP Phase 6 historical simulations (CMIP6, Eyring et al.,
2016) to represent all historical natural and human-induced external forcing.

Beyond mere correlation, causal discovery aims to learn the underlying causes and effects of the climate system (Runge
et al., 2023). Similar to our previous research (Karmouche et al., 2023), in this study we apply a causal discovery algorithm
90 to understand the regime-dependent causal networks connecting coupled and atmospheric modes of climate variability over
the Atlantic and Pacific. While Karmouche et al. (2023) addressed teleconnections happening at yearly-interannual to decadal
lags, this paper focuses on the seasonal to interannual timescale. The study encompasses a causal analysis of reanalysis data
to investigate the distinctive regimes of teleconnections during two historical periods as suggested by Meehl et al. (2021);



95 Park et al. (2023), namely the Pacific-driven regime (1950-1983) and the Atlantic-driven regime (1985-2014). Pacemaker
simulations are also used to explore the role of ENSO on North Pacific and North Atlantic teleconnections before and after
removing the externally forced signal. Finally, to show that Atlantic-Pacific interactions happen naturally, even in the absence
of external influences, we show results using a pre-industrial control run.

2 Data

2.1 Reanalyses datasets

100 To calculate SST-based indices over the Atlantic and Pacific during the observed historical 1950-2014 period, we use the
Hadley Centre Sea Ice and Sea Surface Temperature (HadISST, Rayner et al., 2003) dataset. We also use sea level pressure
(SLP) and zonal wind component (U) at 925 hPa obtained from the National Center for Environmental Prediction-National
Center for Atmospheric Research reanalysis 1 dataset (NCEP-NCAR-R1 Kalnay and Joseph, 1996) to calculate indices for the
atmospheric modes (NAO and PNA) and the Pacific Walker Circulation (PWC).

105 2.2 Pacific pacemaker simulations

To address the effect of external forcing on the Atlantic-Pacific interactions, we utilized a 10-member ensemble of the Com-
munity Earth System Model 2 (CESM2 ?) in which observed SSTAs in the eastern tropical Pacific were nudged to National
Oceanic and Atmospheric Administration (NOAA) Extended Reconstruction Sea Surface Temperature version 5 (ERSSTv5)
data during 1880-2019. Similar to reanalyses datasets (see Sect. 2.1), the analysis of Pacific pacemaker simulations focuses
110 on the period from 1950 to 2014. To preserve the mean state and biases of the model, the SST nudging was only applied to
the anomalies, not the total SST. The ensemble includes all CMIP6 time-varying external, natural, and anthropogenic forc-
ings, using historical forcings prior to 2014 and SSP3-7.0 forcing thereafter. Similarly to reanalysis data, we extract surface
temperature (TS), SLP, and U variables. The complete description and documentation of the Pacific pacemaker dataset are
available on the Climate Variability and Change Working Group's (CVCWG) webpage ([https://www.cesm.ucar.edu/working-
groups/climate/simulations/cesm2-pacific-pacemaker](https://www.cesm.ucar.edu/working-
groups/climate/simulations/cesm2-pacific-pacemaker), DOI: 10.26024/gtrs-tf57, last access: 01.04.2023).

2.3 Pre-industrial control run

To further examine the interactions between the Atlantic and Pacific modes of internal variability under unforced scenarios, we
use 120 years of the CESM2 pre-industrial control (representative of the period prior to 1850, Eyring et al., 2016) to extract
monthly averages for the same variables as in the pacemaker simulations and reanalysis (TS, SLP, U). We use the CESM2
120 model for its remarkable simulation of ENSO characteristics (Danabasoglu et al., 2020; Deser et al., 2020; Capotondi et al.,
2020; Chen et al., 2021) and also to facilitate the comparison with the pacemaker ensemble results.



2.4 Indices

We calculate the indices for TNA, Niño3.4, PNA, NAO, and the PWC with respect to 1950-2014 climatology as follows:

- 125 – TNA Index is the area-weighted monthly SSTAs over the North Tropical Atlantic region 5.5–23.5 N, 58 W–15 W (Enfield et al., 1999).
- Niño3.4 Index is the area-weighted monthly SSTAs over the equatorial pacific region 5°N–5°S, 170 W–120 W (Trenberth, 1997).
- PNA Index is the leading EOF of (seasonally averaged and area-weighted) SLP anomalies over the Pacific North America region 20–85 N, 120 E–120 W (Wallace and Gutzler, 1981).
- 130 – NAO Index is the leading EOF of (seasonally averaged and area-weighted) SLP anomalies over the North Atlantic region 20–80°N, 90°W–40°E (Hurrell and Deser, 2010).
- PWC_u as an index for the PWC and is defined as the monthly zonal wind anomaly at 925 hPa (or nearest available level for pacemaker simulations) over the equatorial pacific region (6°N–6°S, 180°–150°E, following Chung et al., 2019), where negative (positive) values indicate anomalous easterly (westerly) winds that imply a strengthening (weakening) of
135 the PWC.

We also use indices for AMV and PDV to illustrate the decadal imprint of internal variability over the Atlantic and Pacific during the pre-industrial run, a proxy for the long-term physical state of the two basins. Here the AMV and PDV indices are calculated as follows:

- 140 – AMV Index (sometimes referred to as the AMO index) is defined as monthly SSTAs averaged over the North Atlantic region (0–60 N, 80–0 W) minus the global mean (70 N–60 S, effectively detrending the data, see Trenberth and Shea, 2006).
- PDV Index (sometimes referred to as the PDO index) is defined as the standardized principal component (PC) time series associated with the leading EOF of area-weighted monthly SSTAs over the North Pacific region (20–70 N, 110 E–100 W) minus the global mean (70 N–60 S, effectively detrending the data, see Mantua et al., 1997).

145 3 Methodology

3.1 Separating internal variability from the externally forced components

To isolate internal variability from the Pacific pacemaker simulations, we first calculate a multi-ensemble mean (MEM) for each variable, representing an estimate of the externally forced component. This is done by averaging three CMIP6 historical large ensemble means (with different numbers of ensemble members): CESM2 (11 members), MIROC6 (50 members), and



150 UKESM1-0-LL (16 members). These models were chosen to represent the MEM, since they realistically simulate the spa-
 tiotemporal characteristics of the major modes of climate variability (notably ENSO and North Atlantic SST modes) during
 the historical period (Phillips et al., 2020; Fasullo et al., 2020; Karmouche et al., 2023). Moreover, to detect changes in various
 climate phenomena, the required number of members in an ensemble simulation may differ. Forced changes in ocean heat
 content can be detected with only a few members, while changes in atmospheric circulation or extreme precipitation and tem-
 155 perature may need 20-30 members (Deser et al., 2012; Tebaldi et al., 2021; Smith et al., 2022). Detecting forced changes in the
 characteristics of internal variability, such as its amplitude, spatial pattern, and remote teleconnections, may require even larger
 ensembles (Milinski et al., 2019; Smith et al., 2022; O'Brien and Deser, 2023; Deser and Phillips, 2023). The idea behind
 estimating the forced response from three different large ensembles with different numbers of realizations is to reduce any
 biases originating from the model's own representation of CMIP6 forcing and/or from the ensemble size. Because each of the
 160 10 members in the pacemaker ensemble is subjected to the same CMIP6 time-varying external forcing, we assume that MEM
 is the response to external forcing such as GHG-induced warming trends, solar radiation, volcanic activity, land use changes,
 and anthropogenic aerosols. Consequently, the discrepancies in each pacemaker simulation relative to MEM can be attributed
 to internal variability. Therefore, for a given variable X ($X = SST, U, SLP$), we can express the separation in a pacemaker
 simulation i as:

$$165 \quad X_i = X_{MEM} + X_{internal(i)}, \quad i = 1, 2, \dots, 10 \quad (1)$$

where X_{MEM} is the forced component estimated from the CMIP6 MEM and $X_{internal(i)}$ is the residual of the original X_i minus
 the forced response X_{MEM} , which varies among different members and shows the component associated with isolated internal
 variability. This is similar to methods from Wu et al. (2021), but using the CMIP6 MEM instead of the pacemaker ensemble
 mean to quantify the forced component.

170 To isolate the internal variability in observations and the pacemaker simulations following Eq. (1), we subtract the MEM for
 SST, SLP, and U from observations and each pacemaker simulation before calculating the indices above. Figure 1 illustrates
 the standardized seasonally averaged time series of Niño3.4 (a), TNA (b), PNA (c), NAO (d), and PWC_u (e) indices from
 observations for the 1950-2014 period. For each index, the time series in black represents the original indices from HadISST
 (a,b) and NCEP-NCAR-R1 (c-e), as mixed signals including external forcing (non-linear trends). The time series in green
 175 show the indices after subtracting MEM (producing an isolated internal variability). The difference that denotes the effects of
 external forcing is shown in red. Based on Fig. 1, there are two indices that expose positive trends represented by external
 forcings, namely Niño3.4 (a) and TNA (b). The rest of the analyzed indices do not show distinctive trends nor significant
 effects of external forcing.

3.2 PCMCI+ algorithm for causal discovery

180 Similar to methods from Karmouche et al. (2023), we use the PCMCI+ causal discovery algorithm, part of the freely available
 Tigramite python package (<https://github.com/jakobrunge/tigramite>, last access: 03.07.2023) to efficiently estimate causal
 networks from time series datasets (Runge et al., 2019), and detect lagged ($\tau > 0$) and contemporaneous ($\tau = 0$) causal links



Observed time series of Niño3.4, TNA, PNA, NAO, and PWC_u

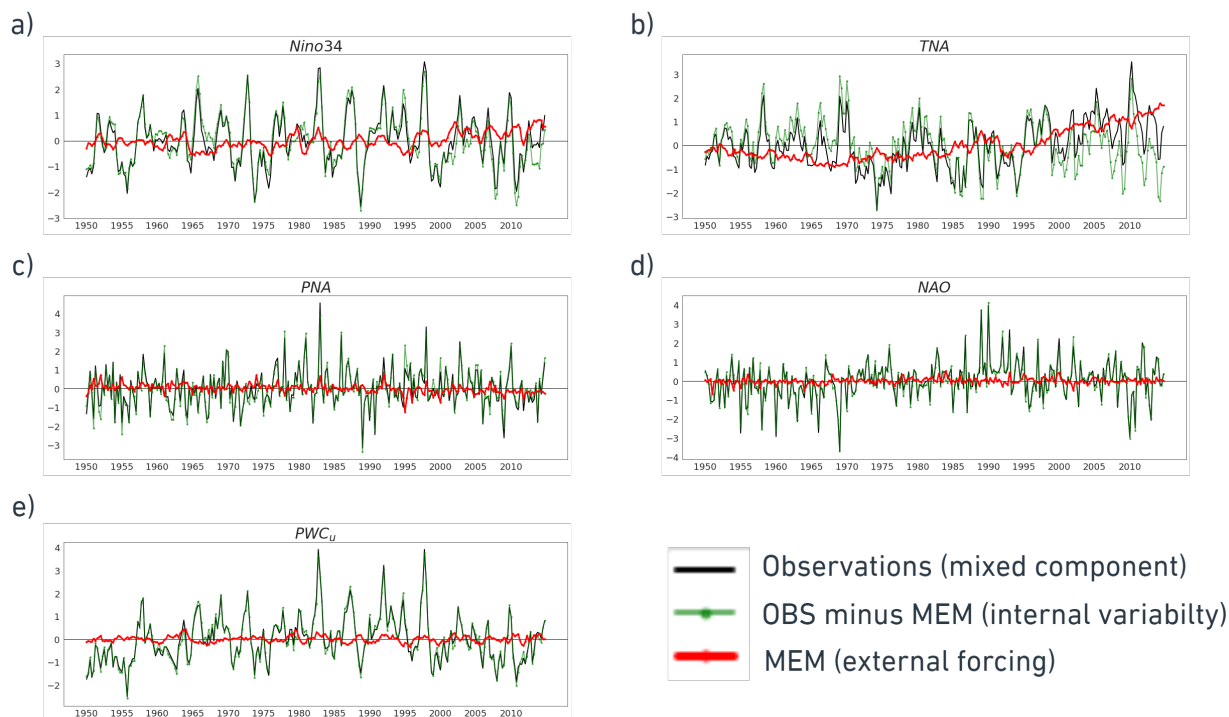


Figure 1. Standardized seasonally averaged time series of a) Niño3.4, b) TNA, c) PNA, d) NAO, and e) PWC_u during the observed 1950-2014 period. Unit for the standard deviations are [°C] in a and b, [Pa] in c and d, and [m.s⁻¹] in e. The time series in black represent the mixed signal from indices calculated using HadISST (a,b) and NCEP-NCAR Reanalysis-1 (c-e). The time series in green are calculated after subtracting the CMIP6 external forcing represented by MEM following Eq. 1 (see Sect. 3.1). In each panel, the red line denotes the difference between the black and green line at each time step, representing the varying effect of subtracting MEM on each index.

(Runge, 2020), where τ stands for the time lag. The full description of the method and pseudo code, along with explanations of the underlying assumptions for causal interpretation, can be found in Runge et al. (2023) and Runge (2020), respectively.

185 Crucially, to interpret obtained links in PCMCi+ as causally directed, the method assumes that no unobserved confounders exist.

The PCMCi+ algorithm consists of two main phases: skeleton discovery and orientation. The skeleton discovery phase starts with the PC1 Markov set discovery algorithm, which is based on the PC algorithm (Peter Spirtes and Clark Glymour), to test for conditional independence of pairs of variables, and it is followed by a momentary conditional independence (MCI) test to remove spurious links due to contemporaneous confounders (Runge, 2020). The orientation phase orients contemporaneous links based on unshielded triples, and the resulting graph contains directed lagged and contemporaneous links as well as unoriented contemporaneous adjacencies (Markov equivalence) or conflicting adjacencies (see rules R1–R3 in Runge, 2020).



The resulting links are then visualized as a process graph that summarizes causal dependencies and their time lags. Here, we estimate the link strengths as standardized (causal) regression coefficients (Runge et al., 2015) using a linear mediation
195 model from the actual parents estimated by PCMCI+. More precisely, we estimate each variable X_t^j on its parents $pa(X_t^j)$. Then, the regression coefficients corresponding to each parent provide a link coefficient with a causal interpretation under the above assumptions. Considering X and Y are variables represented by their time series, and the time lag τ , if we assume causal sufficiency and that the linear model is suitable, then the link coefficient (link coeff.) of $X_{t-\tau}$ to Y_t obtained from standardized time series tells us how much the expected value of Y_t (measured in standard deviation units) will change if $X_{t-\tau}$
200 is changed by one standard deviation. Note that the PCMCI+ resulting graphs may contain unoriented as well as conflicting links at lag zero (e.g. due to Markov equivalence and conflicting orientation rule applications). Here we orient these links to satisfy a (fully-oriented) Directed Acyclic Graph (DAG) based on the direction in which they most appeared in all instances of that particular contemporaneous link across the CESM2 pacemaker ensemble during each regime. The set of directions learned from the majority ruling is used to direct unoriented links during the reanalysis and the pre-industrial control runs as
205 well. Such adjustment is practiced while ensuring no occurrence of contemporaneous cycles. Table S1, part of Supplementary Material, shows the originally unoriented contemporaneous links, their instances, their new directions, and the basis on which the directions were decided.

3.2.1 Proof of Concept: the 1997/1998 El Niño

The ENSO phenomenon has been a subject of intense scientific interest due to its profound impacts on global climate pat-
210 terns. Among the ENSO events, the El Niño of 1997/1998 stands out as one of the most powerful and influential episodes in recorded history. The processes and feedbacks involved with this event are relatively well understood and documented (e.g. McPhaden, 1999; Lengaigne et al., 2003). Thus, as a proof of concept for our methodology, we apply causal discovery to analyze this event and to physically interpret it in the context of well-known processes. This will provide insight to point toward the causal analysis in this paper of the less well-understood interactions between the Pacific and the Atlantic. Through the
215 application of the PCMCI+ causal discovery algorithm, we identify potential cause-and-effect relationships among the selected variables, shedding light on the intricate interactions that contributed to the onset and intensification of the 1997/1998 El Niño event. Candidate variables for this case study, which have been used in previous studies (Trenberth, 1997; Neelin et al., 1998; McPhaden, 1999; Lengaigne et al., 2003; Wang, 2018) and thus applied here, include the SSTAs over the Niño3.4 region (SST Niño3.4), precipitation over the central Pacific (Precip CPAC), the wind stress over the west Pacific ($Wind_{Stress}$ WPAC), the
220 east-west SLP anomaly gradient (SLP_{grad} EPAC-WPAC), and the depth of thermocline in the east Pacific ($Tcline_{Depth}$ EPA). We extract these variables as monthly averages between January 1995 and December 1999 from NCEP-NCAR-R1, HadISST, and two reanalysis datasets from the European Centre for Medium-Range Weather Forecasts (ECMWF), namely, the Ocean Reanalysis System 5 (ORAS5, Copernicus Climate Change Service, Climate Data Store, 2021) and ERA5 (Hersbach et al., 2023) datasets. This means that the PCMCI+ data frame in this section has a length of 60 time steps (months) with 5 variables,
225 which are listed in Table 1 with their respective details.



Table 1. Climate variables used in the 1997/1998 El Niño case study

Variables (nodes)	Dataset	Definition	Region
SST Niño3.4	HadISST	SSTAs over the Niño3.4 region [$^{\circ}\text{C}$]	5°S-5°N, 170°W-120°W
Precip CPAC	ERA5	Central Pacific Precipitation Anomalies [m]	5°S-5°N, 170°W-120°W
Wind _{Stress} WPAC	ORAS5	West Pacific Wind Stress Anomalies [$N.m^{-2}$]	5°S-5°N, 140°E-170°E
SLP _{grad} EPAC-WPAC	NCEP Reanalysis 1	East-West Sea Level Pressure Anomaly Gradient [Pa]	[5°S-5°N, 100°E-160°E] minus [5°S-5°N, 100°W-160°W]
Tcline _{Depth} EPAC	ORAS5	Depth of 20°C Isotherm in the Eastern Pacific [m]	5°S-5°N, 150°W-120°W

The Tigramite package offers the ability to plot causal networks where nodes represent the time series associated with each climate variability index. Node colors indicate the coefficient of the self-links (auto-coefficient) for each time series, and the colors of the links (arrows) denote the linear link coefficients, with blue indicating opposite-sign (negative) inter-dependency and red indicating same-sign (positive) inter-dependency strength. The link-associated time lags are shown as small labels on the curved links. If a lagged link is detected more than once, the indicated lags are sorted by strength (sorted by the absolute value of the link coefficient). During this proof-of-concept section, we estimate dependencies only for lags between 1 and 3 months ($\tau_{min} = 1, \tau_{max} = 3$). This is due to data availability and also because the inter-dependencies happening on a daily-to-weekly timescale are not within the scope of this paper. For this ENSO study, the PCMCi+ algorithm detected causal links that can be summarized through the causal network shown in Fig. 2. We show the time series of each variable next to each node shown in the causal network.

The results obtained from the PCMCi+ algorithm confirm previous insights into the mechanisms leading to the 1997/1998 El Niño event by identifying significant causal links among the variables. One crucial node with multiple originating links is Wind_{Stress} WPAC, indicating its central role in driving various aspects of the 1997/1998 El Niño phenomenon.

The links from Wind_{Stress} WPAC are as follows:

1. Wind_{Stress} WPAC \rightarrow Tcline_{Depth} EPAC with a 1-month lag and as same-sign response. This link indicates that the westerly wind burst in the West Pacific contributed to an increase in the thermocline depth in the Eastern Pacific during the following month (associated with an eastward propagating downwelling Kelvin wave in the ocean as previously

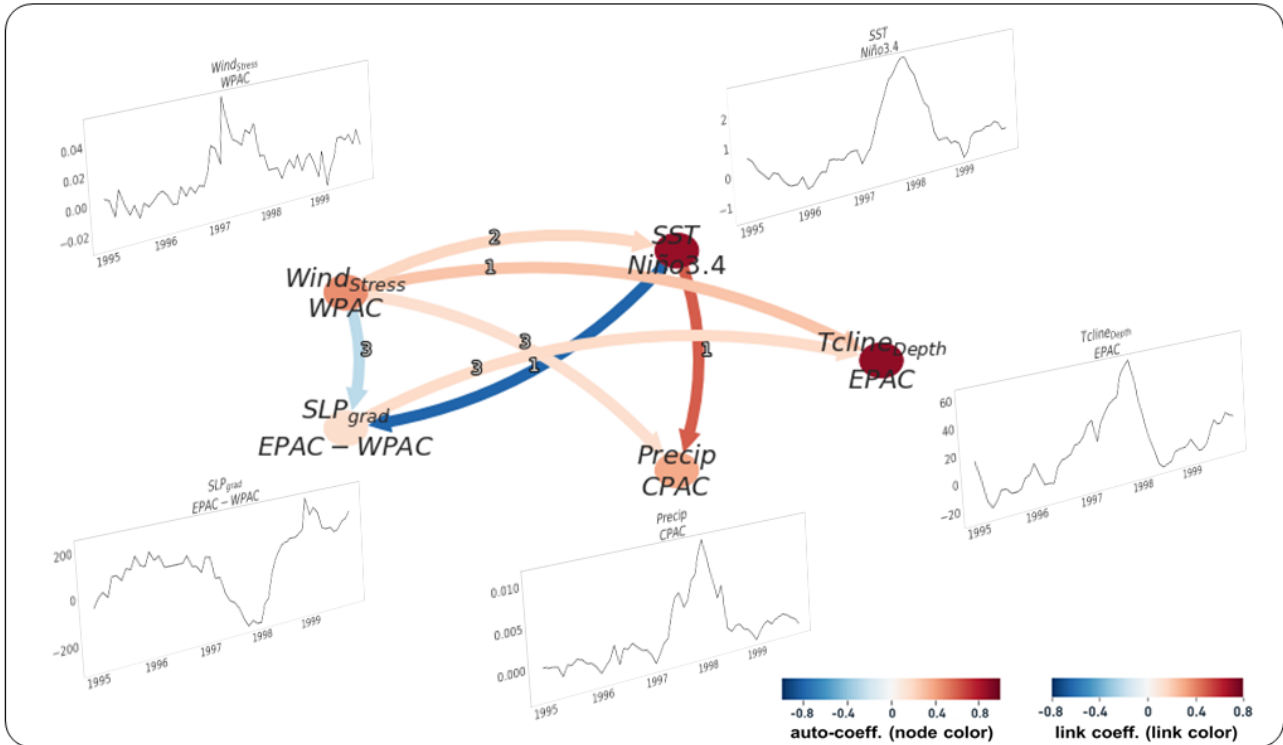


Figure 2. Causal networks representing lagged causal links between the variables in Table 1 for the 1997-1998 El Niño event. Constructed by applying PCMCi+ on the detrended time series of each variable between January 1995 and December 1999. Nodes represent the time series associated with each climate variable (see node labels and details in Table 1). Node colors indicate the self-link coefficients of each time series (auto-coeff, see color bar), and the color of the links denotes the linear link coefficient (link coeff, see color bar). The link-associated time lags (unit=1 month) are shown as small labels on the links.

documented). As the thermocline deepens in the east, upwelling brings up warmer water from the thickened thermocline, contributing to the warming of SSTs in the central and eastern equatorial Pacific.

245

2. $Wind_{Stress} WPAC \rightarrow SST Ni\acute{o}3.4$ with a 2-month lag and as same-sign response. This link indicates that as the wind stress over the West Pacific increases, it causes the SST anomalies over the Niño3.4 region to increase with a lag of 2 months. The deepening of the thermocline in the east and the reduction in the upwelling of colder waters further contribute to the anomalous warming of SSTs in the central and eastern equatorial Pacific.

250

3. $Wind_{Stress} WPAC \rightarrow SLP_{grad} EPAC-WPAC$ with a 3-month lag and as opposite-sign response. This link indicates that the westerly wind burst in the West Pacific contributes to a three-month lagged decrease in the sea-level pressure gradient between the East and West Pacific. The decreasing SLP gradient means that the sea level pressures over the West Pacific become anomalously higher than those in the East Pacific, contributing to changes in atmospheric circulation and the thermocline depth.



255 4. $Wind_{Stress}$ WPAC \rightarrow Precip CPAC with a 3-month lag and as same-sign response. The link indicates that the anomalous increase in wind stress in the West Pacific contributes to an increase in Central Pacific precipitation after three months of the wind burst. Although no link originating from Precip CPAC was detected, the shift in precipitation patterns further amplifies the anomalous warming in the Niño3.4 region due to reduced upwelling and the Bjerknes feedback.

The links from SST Niño3.4 are as follows:

260 1. SST Niño3.4 \rightarrow Precip CPAC with a 1-month lag and as same-sign response. This link means that the rising temperatures in the Central Pacific Niño3.4 region contributed to the increased rainfall over the same region after a one-month lag. The changes in precipitation patterns further affect the atmospheric and oceanic conditions, reinforcing the warming in the Niño3.4 region.

265 2. SST Niño3.4 \rightarrow SLP_{grad} EPAC-WPAC with a 1-month lag and as opposite-sign strong response. This link suggests that the rising temperatures over the Niño3.4 region greatly decrease the East-West sea-level pressure gradient. This reduction in the SLP gradient contributes as an indicator of a weakening of the Pacific Walker Circulation, further impacting atmospheric and oceanic conditions during the El Niño event.

The link from SLP_{grad} EPAC-WPAC is as follows:

270 1. SLP_{grad} EPAC-WPAC \rightarrow $Tcline_{Depth}$ EPAC with a 3-month lag and a same-sign response. This link suggests that the decreasing East Pacific SLP anomalies (compared to the West Pacific), associated with both rising SSTs in the Niño3.4 region and the preceding increased Wind Stress over the West Pacific, contribute to a decrease in the thermocline depth over the East Pacific. However, this link's interpretation is tricky, as it suggests that the SLP gradient decreasing would cause the thermocline to become shallower after three months, which is opposite to the one-month lagged strong increase due to the West Pacific wind burst. This link color, on the other hand, suggests that the effect of $Wind_{Stress}$ WPAC \rightarrow $Tcline_{Depth}$ EPAC is stronger in driving changes in the thermocline depth during the El Niño event than the 3-month lagged SLP_{grad} EPAC-WPAC \rightarrow $Tcline_{Depth}$ EPAC link.

To summarize, a causal analysis has been applied to the El Niño event of 1997/1998 to demonstrate the utility of such an analysis in quantifying the connections between physical processes. Previous results are confirmed by this causal analysis in that the westerly wind burst event in the western equatorial Pacific in March triggered an eastward traveling downwelling Kelvin wave in the ocean that deepened the thermocline in the east and shallowed it in the west. As SSTs warmed in the eastern equatorial Pacific, trade winds weakened. This weakening reduced the upwelling of cold, nutrient-rich waters in the eastern Pacific and instead brought up relatively warmer water from the thickened thermocline, contributing to the warming of SST in the Niño 3.4 region. The identified causal links align with the mechanisms involving the $Wind_{Stress}$ WPAC influencing thermocline depth, and leading to anomalous warming in the Niño3.4 region, in agreement with extensive previous studies (McPhaden, 1999; Lengaigne et al., 2003). Furthermore, the East-West SLP anomalies and anomalous shifts in precipitation patterns are shown to be greatly affected by the SST variations in the central east Pacific as hypothesized, and this further contributes to the intensification and maintenance of the 1997/1998 El Niño event.



With this demonstration of the utility of causal analysis in quantifying connections between phenomena that represent previously documented physical processes, we now apply the causal methodology to the less well-understood problem of the nature of the connections between the Pacific and Atlantic.

3.2.2 PCMCI+ application to Atlantic-Pacific connections

On the time resolution of the PCMCI+ data frames used in Sect. 4, we note that we use seasonally averaged time series of each index (TNA, Niño3.4, PNA, NAO, and the PWC_u) with four seasons (time steps) per year, as averages of January-February-March (JFM), April-May-June (AMJ), July-August-September (JAS), and October-November-December (OND). For the parameter settings of the PCMCI+ algorithm, we set the maximum time lag to 8 time steps ($\tau_{max} = 8$ [seasons]), meaning that we only investigate teleconnections within a maximum of two-year time lag. Additionally, we also look at contemporaneous links detected within the same season ($\tau_{min} = 0$). These contemporaneous inter-dependencies that happen with no time lag (i.e., $\tau < 1$) are shown as straight links on the causal networks (Sect. 4). The significance level of the MCI partial correlation tests α_{pc} is set to 0.2 to account for the short sample size. It is important to note that the networks are only causal with respect to the analyzed variables, and more advanced methods that can deal with hidden variables (Gerhardus and Runge, 2020) may not be suitable for short sample sizes.

4 Results

4.1 Observed teleconnections in Reanalysis datasets

4.1.1 Correlation and regression patterns

To demonstrate the relationships between Atlantic and Pacific SST modes and to estimate the effect of removing the externally forced signal (represented by MEM, for more details see Sect. 3.1) from the original SSTs, we first calculate Pearson's correlation between global SSTAs with SST-derived indices based on the original HadISST dataset.

Figure 3 displays the regression patterns of global SSTAs during two distinct regimes: the Pacific-driven 1950-1983 period (Fig. 3a and b) and the Atlantic-driven 1985-2014 period (Fig. 3c and d). The analysis in Fig. 3 focuses on the relationship between SSTAs and two key climate indices (namely Niño3.4 and TNA indices) using the original SST signal, hypothesized to contain influences of both internal variability and external forcing (as discussed in Sect. 3.1 and seen in Fig. 1a and b). Figure 4, on the other hand, shows the same analysis but after isolating the internal variability component of the SST modes and anomalies by subtracting MEM from the original SST fields following Eq. (1). For both Fig. 3 and 4, the top panel (a) illustrates Pearson's correlation coefficients and regression coefficients between detrended global SSTAs and the standardized Niño3.4 index for the period 1950-1983, based on HadISST data. Similarly, the second panel (b) presents the same correlation and regression analysis but with the standardized TNA index instead of Niño3.4. The bottom panels (c) and (d) replicate the analyses from panels (a) and (b) but for the period 1985-2014. To visualize the impact of subtracting MEM, the reader can

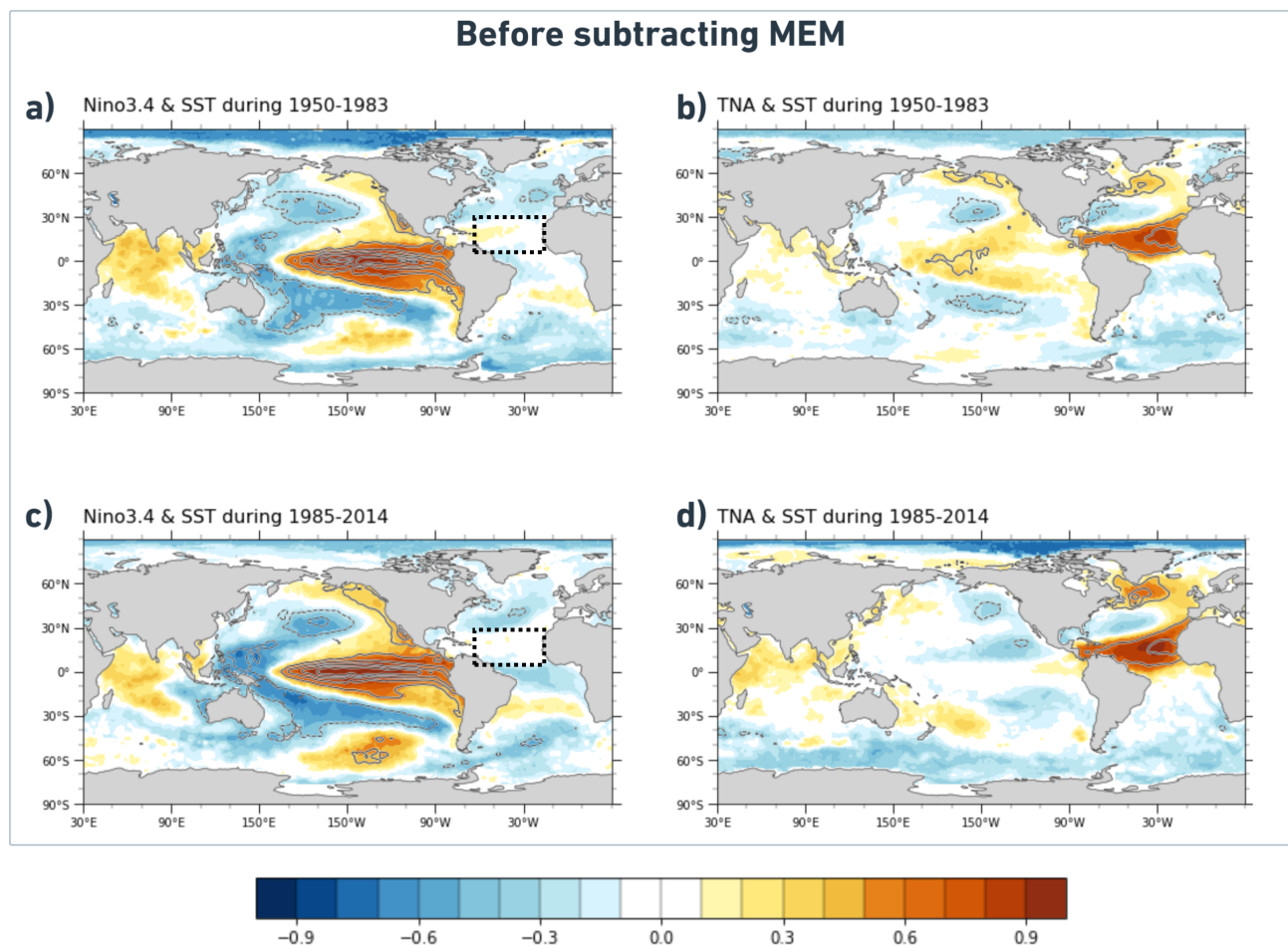


Figure 3. Regression pattern of global SST anomalies (SSTAs) onto Niño3.4 index (a,c) and TNA index (b,d) during both periods: 1950-1983 (top) vs 1985-2014 (bottom). a) Pearson's correlation coefficients (shadings) and regression coefficients (contours) of de-trended global SSTAs with the standardized Niño3.4 index based on HadISST data during 1950-1983. b) Same as (a) but showing the SSTAs correlation and regression with the standardized TNA index instead of Niño3.4. c) Same as (a) but for the 1985-2014 period. d) Same as (b) but for the 1985-2014 period. White-shaded areas indicate weak correlations (between -0.1 and 0.1). The contour interval is 0.2 (°C) with dashed (solid) contours indicating regions with negative (positive) regression coefficients. Global SSTAs are detrended by removing the global mean at each time step. For convenience, the dashed black box shows the considered TNA region.

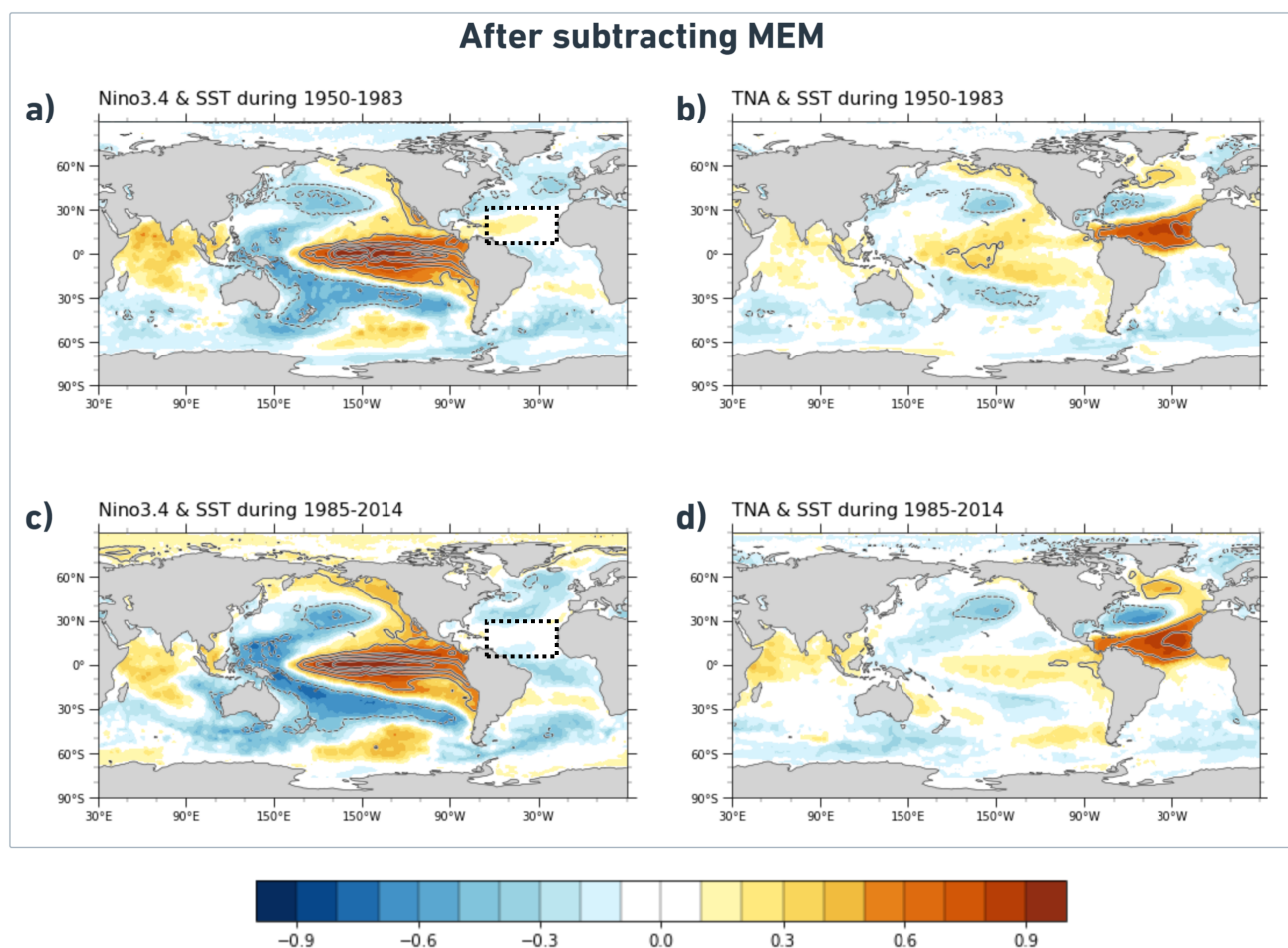


Figure 4. Similar to Fig. 3 but after removing the externally forced signal represented by MEM following Eq. (1) (see methods Sect 3.1.). All SST fields have the CMIP6 MEM subtracted prior to calculating anomalies and performing the regressions.



compare one panel from Fig. 4 to its respective panel in Fig. 3.

320 **SSTAs regression onto the Niño3.4 index.**

Before removing external forcing, during the 1950–1983 period (Fig. 3a), we find weak correlations between the Niño3.4 index and SSTAs over most of the Atlantic with negative values extending from the European west coast and decaying north of the TNA region (black dashed box in Fig. 3a). Within this TNA region, there are weak positive correlations extending from the Gulf of Mexico and decaying around the center of the TNA region. This positive relationship is consistent with several
325 previous studies (Enfield and Mayer, 1997; Klein et al., 1999; García-Serrano et al., 2017; Jiang and Li, 2019) that suggest warm (cold) SSTAs develop over the TNA region and peak during the spring and summer following an El Niño (La Niña) winter (Park et al., 2023). These positive values vanish when analyzing the 1985-2014 period (Fig. 3c), where the TNA region shows mainly values between -0.1 and 0.1 for the Niño3.4 index correlation with the SSTAs over that region (see the black dashed box in Fig. 3c). In the North Pacific, both periods show positive correlations extending along the west coast of North
330 America, and negative correlations in the central North Pacific. This horseshoe-like pattern is consistent throughout all SSTA-Niño3.4 regression maps (panels a and c in Fig. 3 and Fig. 4). Comparing Fig. 4a to Fig. 3a, we conclude that although the positive correlations of tropical Atlantic SSTAs with the Niño3.4 index slightly increased when subtracting MEM during the Pacific-driven 1950-1983 period, the impact of removing the externally forced signal is not pronounced. This conclusion also holds for the SSTA-Niño3.4 correlations during the 1985-2014 regime as there are no major differences between the TNA box
335 (dashed box) in Fig. 4c compared to the one in Fig. 3c.

SSTAs regression onto the TNA index.

During the first period (1950-1983), the results suggest no major difference in the relationship between the TNA index and North Pacific SSTAs before and after removing external forcing. The correlation maps for the Pacific-driven regime (Fig. 3b and 4b) show mainly positive values in the central equatorial Pacific and negative values in the central North and central South
340 Pacific, similar to the symmetric horseshoe pattern observed from the Niño3.4 regressions shown in Fig. 3a and 4a. Conversely, the subsequent 1985-2014 Atlantic-driven period, where externally forced warming projects greatly onto the Atlantic SST changes (Mann et al., 2014; Klavans et al., 2021, 2022), Fig. 3d shows negative correlation values of TNA index with SSTAs over the eastern Tropical and North Pacific. However, the removal of the external forcing resulted in a strengthened dipole SSTA pattern over the North Atlantic and weak positive correlations over the central and eastern equatorial Pacific (Fig.
345 4d). The removal of external forcing suppressed the negative relationship between the TNA index and SSTAs over the tropical and northeastern Pacific during the 1985-2014 period (Fig. 4d). It is also important to highlight that the impact of external forcing is much more pronounced during 1985-2014, given the clear differences in the Pacific sector between the correlation maps in Fig. 3d and 4d, and which falls in agreement with previous studies (Meehl et al., 2013; Dong et al., 2014; Kucharski et al., 2016; Dong and McPhaden, 2017; Meehl et al., 2021). This suggests that external forcing might have played a major role in
350 the recent effect of the Atlantic on the Pacific. However, the nature of these connections remains unclear. Next, the causal discovery methodology will be applied to better quantify these connections to provide insights into the relevant physical processes.



4.1.2 Causal networks

To investigate the teleconnections during the two periods from a causal discovery perspective, Fig. 5 demonstrates causal networks of Atlantic-Pacific teleconnections based on indices from Sect. 2.4 from the Reanalyses datasets (Sect. 2.1). The left panels in Fig. 5 (a,c) show the resulting causal networks during the 1950-1983 Pacific-driven period, while the panels on the right (b,d) show the networks for the 1985-2014 Atlantic-driven period. For each period, the panel on top (a,b) represents the original observed signal (corresponding to the black curve in Fig. 1). The bottom panel shows the networks where indices have been calculated after subtracting the MEM, effectively isolating internal variability (corresponding to the green curve in Fig. 1). In the bottom panels (c) and (d) the MEM is subtracted from the reanalyses before PCMCi+ is applied. Picturing Niño3.4, PNA and PWC_u as variables representing the Pacific while TNA and NAO represent the Atlantic, we can, for example, look at how nodes from the Pacific basin are linked to each other and to the Atlantic ones, and vice-versa.

As a general note, based on Fig. 5 (all panels), we detect the extensively studied relationship of ENSO and PWC (Trenberth, 1997; Bayr et al., 2014; Zhao and Allen, 2019), illustrated through the strong positive contemporaneous causal connection from PWC_u to the Niño3.4 ($PWC_u \rightarrow$ Niño3.4 link). We confirm that positive values of PWC_u indicate anomalously weak easterly winds associated with the weakening of PWC and the emergence of El Niño events. With PWC inextricably linked to Niño3.4, a conclusion solidified throughout the results in Sect. 4.2 and 4.3, we consider causal links to and from a PWC_u node to denote a causal relationship associated with ENSO. We also find a weak opposite sign causal response from PWC_u to Niño3.4 at one season lag (Fig. 5a and c).

370 Pacific-driven period 1950-1983

The Pacific-driven 1950-1983 is found to be dominated by a same-sign effect from ENSO on TNA through both tropical and extra-tropical routes. During an El Niño event, the weakened Walker circulation allows an eastward shift in the maximum convection center from the Maritime Continent to the central equatorial Pacific. This tropical convection triggers a poleward-propagating Rossby wave which extends into the midlatitudes, constituting the PNA pattern. This teleconnection linking the equatorial and extra-tropical Pacific is detected as a lagged positive causal link from PWC_u to PNA during 1950-1983 (Fig. 5a and c). The wave pattern associated with PNA contributes to the formation of an anomalous low-pressure center over the southeast United States and the Caribbean. The presence of the PNA pattern results in anomalous southwesterly winds over the TNA region. The negative rainfall anomaly over the western Pacific and the Atlantic region, caused by the reversed Walker circulation during El Niño, plays a role in inducing this anomalous low-pressure center over the southeast United States. Additionally, the suppressed heating response in the Atlantic region, resembling the Gill-like pattern (Matsuno, 1966; Gill, 1980), also contributes to the development of anticyclonic circulation and southwesterly wind anomalies over the TNA region (García-Serrano et al., 2017; Jiang and Li, 2019). The combined effect of these extratropical and tropical routes leads to southwesterly wind anomalies that weaken the northeasterly trade winds, reduce evaporation, and induce SSTA warming over the TNA region (Trenberth, 1997; Wallace and Gutzler, 1981; García-Serrano et al., 2017; Jiang and Li, 2019; Meehl et al., 2021; Casselman et al., 2021; Park et al., 2023). The two routes for the ENSO effect on TNA, which is enhanced during the 1950-1983 period, can be seen through the causal networks in Fig. 5a and c showing two positive (lagged) links from the



Observed teleconnections (1950-1983 vs 1985-2014)

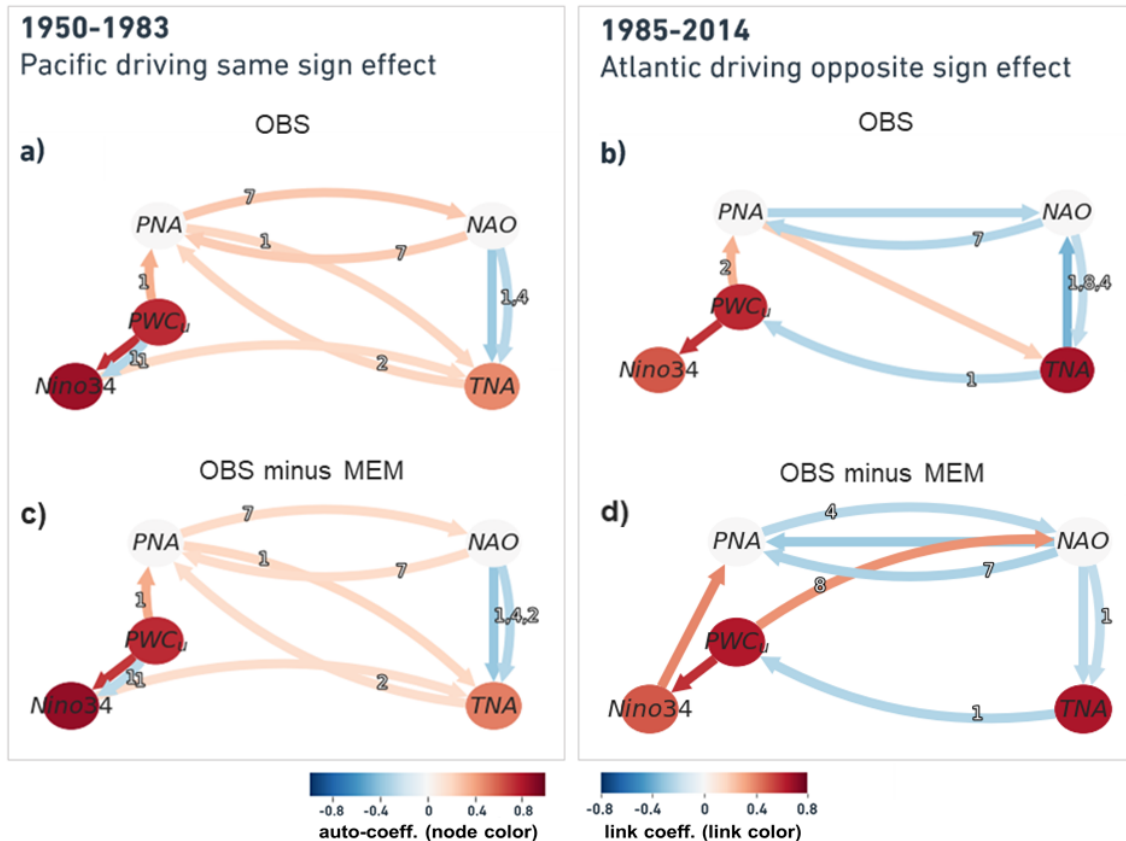


Figure 5. Causal networks representing Atlantic-Pacific teleconnections for 1950-1983 (left column) vs 1985-2014 (right column) in the Reanalyses datasets. (a) Constructed by applying PCMCI+ on the standardized time series of the five seasonally averaged indices calculated from reanalysis datasets for the 1950-1983 period. Nodes represent the time series associated with each climate variability index (see node labels). Node colors indicate the auto-link coefficients (auto-coeff), and the color of the links denote the linear link coefficient (link coeff). The link-associated time lags (unit=1 season) are shown as small labels on the curved links. Straight links show contemporaneous inter-dependencies that happen with no time lag. (b) Same as (a) but for the 1985-2014 period. (c) same as (a), but with indices calculated after removing MEM. (d) Same as (c) but for the 1985-2014 period.

Pacific to TNA: PNA → TNA (1 season) and Niño3.4 → TNA (1 season). The TNA → PNA link in Fig. 5a and c is lagged by two seasons which might suggest that the warming over the TNA region contributes back to anomalous southwesterly winds and maintains the PNA pattern. The Pacific-driven regime's causal graphs show that after El Niño excites PNA, the latter appears to be mutually connected to the NAO with a 7-season lag (PNA → NAO and NAO → PNA links in Fig. 5a and c). These links are however inconsistent with previous studies on the linkage between North Atlantic and North Pacific modes of atmospheric circulation and which suggest contemporaneous negative links between PNA and NAO. Honda et al. (2001)



conducted a study on the period between 1979 and 1994 and discovered a negative correlation (-0.7) between the intensities of the Aleutian and Icelandic lows (low-pressure centers of the PNA and NAO, respectively). Song et al. (2009) concluded that the strongest negative correlations between PNA and NAO occur with no time lag and within a range of 10-day lags. By analyzing reanalysis datasets, Pinto et al. (2011) found no significant anti-correlation between PNA and NAO between 1950 and the mid-1970s, but this was clearly detected during the sub-period 1973–1994. A period of weak PNA-NAO coupling might explain the undetected contemporaneous PNA→NAO negative links during the Pacific-driven period. According to Soulard and Lin (2017), it is the absence of tropical forcing from ENSO that strengthens the relationship between PNA and NAO. On the other hand, observational uncertainty prior to the satellite era can also be a reason that lagged positive links were detected between NAO and PNA instead of contemporaneous negative links. On the Atlantic side, apart from the influence of ENSO and PNA on TNA, NAO is also found to impact the TNA SSTAs (contemporaneous negative NAO→TNA links in Fig. 5a and c). The changes in pressure gradients between the Azores high and the Icelandic low can alter trade winds, heat fluxes, and SSTs. Reduced northeasterly trade winds contribute to trapping warm SSTAs over the TNA region as less latent heat is released into the atmosphere (Cassou and Terray, 2001; Lee et al., 2008). We detect several causal connections between NAO and TNA where the NAO drives changes in TNA, not only contemporaneously but also lagged (NAO→TNA, Fig. 5a and c). This negative relationship of the NAO index with TNA is seen through the negative NAO→TNA links in Fig. 5a and c. Although direct links connecting either Niño3.4 (or PWC_u) to NAO have not been detected during the Pacific-driven regime, the NAO is thought to affect the interplay between ENSO and TNA which is further complicated by the fact that ENSO can also influence the NAO through extratropical pathways (Doblas-Reyes et al., 2017; Casselman et al., 2021). If we consider the causal links that connect the SST modes (Niño3.4 and TNA) directly, or through PWC_u and PNA, then these results support the hypothesis that it was the Pacific SSTs mainly driving the same sign response on the Atlantic SSTs between 1950 and 1983 (Meehl et al., 2021; Park et al., 2023). Overall, comparing Fig. 5a to c reveals a limited effect of external forcing during the first period as no major changes were detected in the causal graph after subtracting MEM.

415 **Atlantic-driven period 1985-2014**

During the second period, the monopole SSTA pattern centered over the TNA region (shown in Fig. 3d) suggests enhanced precipitation there. The Rossby wave energy associated with the enhanced precipitation propagates toward the subtropical Pacific. Combined with the modulated Walker circulation, this induces easterly wind anomalies over the equatorial Pacific, favoring the development of La Niña events (Ham et al., 2013; Park et al., 2022, 2023). This is illustrated in Fig. 5b and d through the 1-season lagged TNA→ PWC_u negative link, an effect that evidently reaches the Niño3.4 node (strong PWC_u →Niño3.4 link). While the atmospheric bridge connecting the equatorial and the extra-tropical Pacific was detected as PWC_u →PNA links in Fig. 5a-c, this was detected as a direct contemporaneous Niño3.4→PNA link when external forcing is removed during the second period (Fig. 5d). Without external forcing, the NAO is found to drive small changes in TNA (Fig. 5d). The contemporaneous TNA-NAO connection is found in the opposite direction during the externally forced Atlantic-driven regime (TNA→NAO, Fig. 5b). The latter is also the strongest occurrence of TNA-NAO links among the results in Fig. 5. The ENSO effect on TNA through the extratropical pathway is still detected when external forcing was not removed. This is seen in Fig. 5b as a contemporaneous link from PNA to TNA in addition to an extratropical PNA teleconnection through PWC_u anomalies



(PNA \rightarrow TNA and PWC_u \rightarrow PNA links). This mild contemporaneous PNA \rightarrow TNA link is suppressed when MEM is subtracted, in contrast to the appearance of a strong 8-season lagged PWC_u \rightarrow NAO link (Fig. 5d) inconsistent with the already
430 proposed negative and short lagged ENSO-NAO relationship (Brönnimann et al., 2007; Brönnimann, 2007). Contrary to the first period, the contemporaneous negative PNA connection to NAO (Honda et al., 2001; Song et al., 2009; Pinto et al., 2011) is detected during the second period (PNA \rightarrow NAO in Fig. 5b and NAO \rightarrow PNA in Fig 5d). Song et al. (2009) explain the anti-correlation they found between day-to-day variability of the Aleutian low and Icelandic low being the result of the anomalous Rossby wave-breaking events associated with the PNA pattern. The paper shows that when the PNA is in a positive (negative)
435 phase, there is more Rossby wave breaking over the North Pacific (Atlantic), which can weaken or split the polar vortex over that region. This can then affect the jet stream and the storm tracks over the North Atlantic, leading to a negative (positive) NAO phase. Lagged negative causal PNA \rightarrow NAO and NAO \rightarrow PNA links are also detected during the 1985-2014 period.

It appears from Fig. 5 that external forcing does not have significant effects on the causal networks from the 1950-1983 regime (Fig. 5c vs 5a), consistent with the SST correlation maps suggesting no major difference before and after subtracting
440 MEM (Fig. 3a vs 4a). Whereas for the following 1985-2014 period, changes were only detected in the tropical/extra-tropical pathways connecting Atlantic and Pacific. The difference between Fig. 3d and 4d hints at a major role played by the externally forced signal in the negative relationship between the TNA index and the tropical east Pacific SSTAs during the Atlantic-driven regime, which is not clearly detected by comparing causal graphs (Fig. 5b vs 5d). Namely, the causal networks show the effect of external forcing as in TNA causing changes in NAO and also in establishing the extra-tropical PNA connection to TNA
445 with no seasonal lag. The latter connection is suppressed when external forcing was removed, in contrast to the appearance of a lagged PWC_u \rightarrow NAO link (comparing Fig. 5b and 5d). Most importantly, inconsistent with the correlation map in Fig. 4d, the one-season lagged negative TNA \rightarrow PWC_u link was still detected, with similar strength (link coeff.), after removing the externally forced signal. It is important to note that this discrepancy, regarding the effect of removing MEM during 1985-2014, was less apparent during a sensitivity test we carried out. There, the analysis of the Atlantic-driven regime was started one year
450 later (1986 instead of 1985) in the observational run and the respective causal graphs revealed that the negative sign response from TNA to PWC was not detected after removing MEM (Supplementary Fig. S1), consistent with the correlation maps from 1985-2014. This further supports the already proposed studies indicating an increasing impact of external forcing on North Atlantic SSTA changes and the associated widespread effects during the most recent decades (Murphy et al., 2017; Klavans et al., 2022; He et al., 2023). In Supplementary Fig. S1, the 8-season lagged PWC_u \rightarrow NAO (featuring in Fig. 5d) was detected
455 before and after subtracting MEM.

The variability of ENSO's relationship to TNA from one regime to another is influenced by the decadal changes in the background mean state. A study by Park and Li (2019) found that the relationship between ENSO and TNA SST is non-stationary and depends on the phase of the AMV. Specifically, when AMV is trending to its negative phase, the impact of ENSO on TNA becomes amplified and has a more prolonged effect. This was the case during the 1950-1983 period when
460 AMV was trending towards its negative phase. During the 1985-2014 period, AMV was trending back from a negative to a positive phase and the opposite was observed (reduced amplitude and shortened effect). The anomalously warm North Atlantic SSTAs during the positive AMV phase favor the strengthening of the PWC, which ultimately brings upwelled cold water



to cool down the central equatorial pacific. The specific contributions of internal variability to these regime changes remain unclear. Zhang et al. (2019) emphasizes the influence of the thermohaline circulation, particularly the Atlantic Meridional Overturning Circulation (AMOC), on the multidecadal changes in Atlantic SSTs. Whereas for the interannual fluctuations, the paper suggests they are primarily driven by wind-induced changes in turbulent heat fluxes. On the other hand, a series of recent papers (Booth et al., 2012; Mann et al., 2014; Bellucci et al., 2017; Watanabe and Tatebe, 2019; Klavans et al., 2022) show growing evidence of an increasing effect of external forcing on the AMV and its lead/lag association with the AMOC. This suggests that internal variability and external radiative forcing contribute to the decadal SST variations over the Atlantic (Meehl et al., 2016; Park et al., 2019; Meehl et al., 2021; Klavans et al., 2022; Park et al., 2023).

4.2 Pacemaker simulations

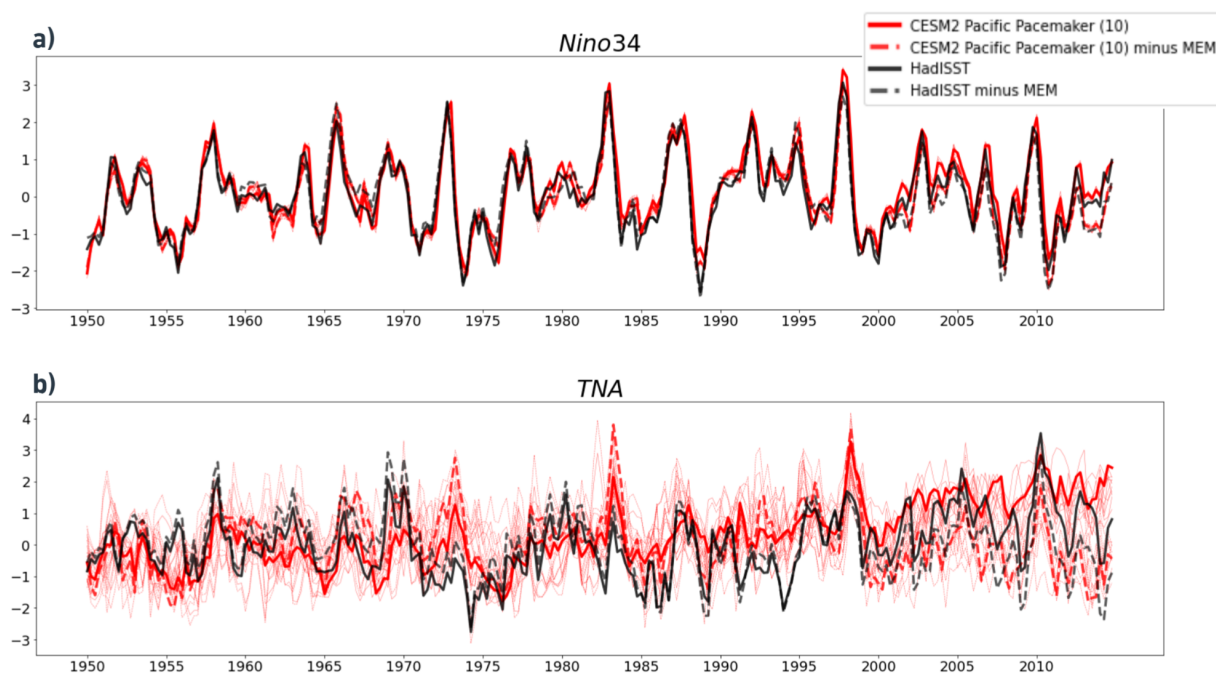


Figure 6. Standardized indices from the Pacific pacemaker ensemble (10 members) together with observations (HadISST) for Niño3.4 (a) and TNA (b). The lines in black show the observed time series from HadISST data before (solid) and after (dashed) subtracting MEM (similar to Fig. 1). The red lines represent the CESM2 Pacific pacemaker ensemble average (10-members) before (solid) and after (dashed) subtracting MEM.

To scrutinize the potential causal dependencies between the modes, we use a 10-member ensemble of the CESM2 Pacific pacemaker simulations (see Sect. 2.2) where Eastern Tropical SSTAs have been nudged towards observed values (maintaining ENSO evolution, Fig. 6a). The rest of the coupled model is free to evolve resulting in different climate variations outside the



Teleconnections in Pacific pacemaker ensemble

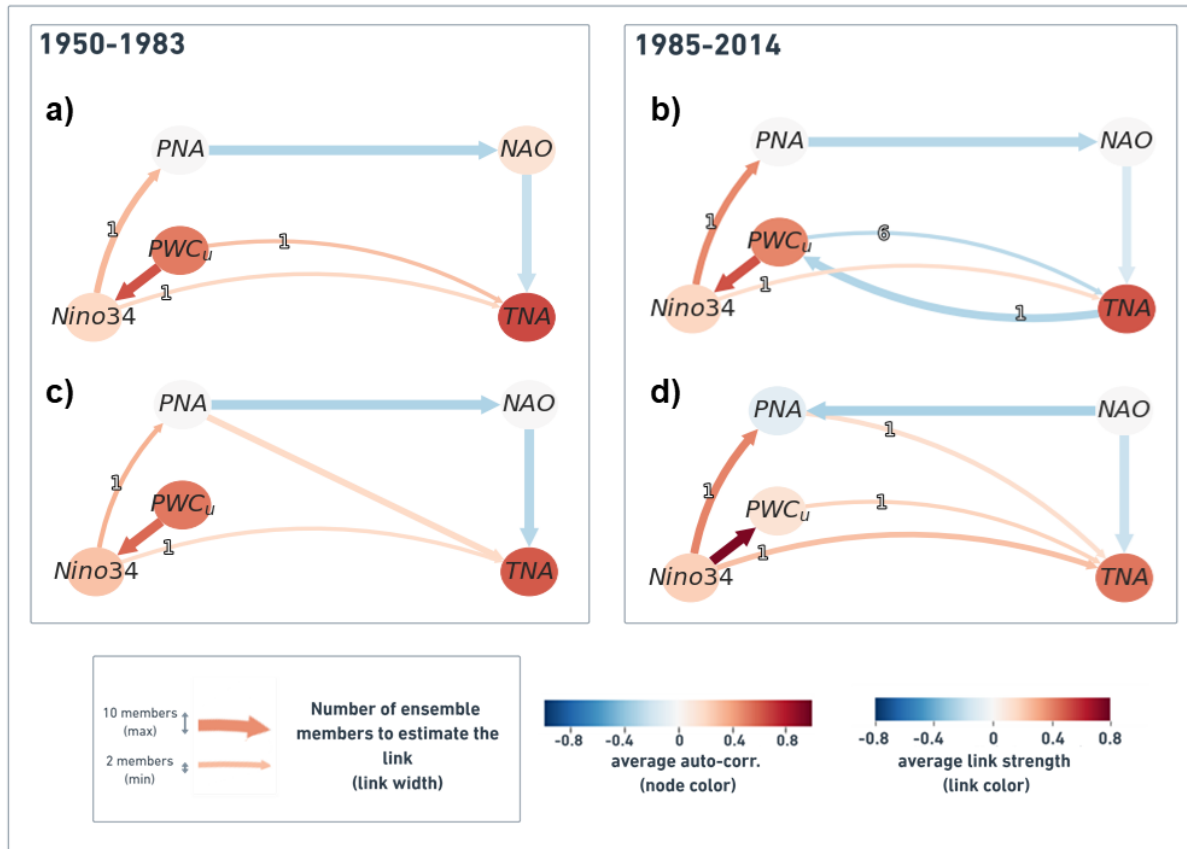


Figure 7. Ensemble summary causal networks and time series from Pacific pacemaker simulations (1950-1983 vs 1985-2014). In panels (a-d), we apply the PCMCI+ on the time series of each simulation before aggregating the 10 causal networks into one. The link width shows the number of simulations that feature that link. The link color shows the mean value of link coefficients averaged over the ensemble members. The node color translates the average auto-coefficient of each time series among the pacemaker ensemble. The link labels provide the median time latency (rounded to the closest integer) for all ensemble members that detect a particular link. In (c) and (d) the MEM is subtracted from every simulation before PCMCI+ is applied. The average (auto-) coefficients were calculated after applying a Fisher z transform. The link labels provide the median time latency (rounded to the closest integer) for all ensemble members that detect a particular link.

475 nudging region depending on the single realizations' own initial conditions. The range of possible outcomes for Atlantic SSTAs is then governed by contributions from internal variability, CMIP6 time-varying external forcing, and the potential cross-basin contributions from the Pacific according to the model's dynamics. The variations of the TNA index in the pacemaker simulations are compared in Fig. 6b to observations (see legend top right), before and after removing the CMIP6 time-evolving external forcing (MEM).



480 Figure 7 is similar to Fig. 5 but shows causal networks based on an ensemble summary of CESM2 Pacific pacemaker
simulations. The causal networks are aggregated based on 10 pacemaker realizations. In the four panels (a-d), we apply the
PCMCi+ on the time series of each simulation before aggregating. The link width indicates the number of simulations that
feature that link (for reference, the width of the link between PNA and NAO in Fig. 7a shows the maximum width, equivalent
to 10 simulations, and the link between Niño3.4 and TNA shows the minimum width, equivalent to 2 simulations). In other
485 words, the more ensemble members were found to estimate the link during that particular run, the thicker the link appeared.
The mean link coefficient value averages all coefficients of that link's instances and the link labels denote the median time lag at
which they were detected. The node color translates the average auto-link coefficient of each time series among the pacemaker
ensemble. In Fig. 7c and d, the MEM is subtracted from every simulation before the causal discovery algorithm is applied.
For simplicity, we directed contemporaneous links based on the most frequent direction in which they are detected within the
490 ensemble (treating each period and scenario separately). We also only took into account links with absolute value coefficients
above the arbitrary threshold of 0.1.

The prominent feature of the causal analysis on the Pacific pacemaker simulations before removing external forcing (Fig.
7a and b) is the ability to distinguish a Pacific-driven period as opposed to an Atlantic-driven one. Similar to observations, the
regression and correlation maps in Fig. 3 and 4, and previously introduced literature (Meehl et al., 2021; Park et al., 2023), the
495 causal networks in Fig. 7 also show the 1950-1983 period was dominated by the equatorial Pacific SSTAs driving a same-sign
effect on the tropical North Atlantic SSTAs and triggering a negative-sign response from the Atlantic onto the Pacific during
the subsequent 1985-2014 period (via $TNA \rightarrow PWC_u$). This is illustrated during the first period through the links originating
from the Niño3.4 (and/or the PWC) node and reaching the Atlantic modes (NAO and/or TNA nodes) either directly (e.g. PWC
 $- TNA$) or potentially through PNA ($Ni\tilde{no}3.4 \rightarrow PNA \rightarrow NAO$, Fig. 7a-c). Both the results from the reanalysis (Fig. 5a) and
500 those from the pacemaker ensemble (Fig. 7a) show positive causal $Ni\tilde{no}3.4 \rightarrow TNA$ links and/or $PWC_u \rightarrow TNA$ during the
Pacific-driven 1950-1983 regime. When MEM is subtracted during this regime (Fig. 7c), contemporaneous $PNA \rightarrow TNA$ links
were also estimated. This means that both the tropical and extra-tropical routes for ENSO effect on TNA are detected during
the Pacific-driven regime (Fig. 7a and c). The 1985-2014 period shows a decay of the extra-tropical pathway (no $PNA \rightarrow TNA$
link in Fig. 7b) and shows that several ensemble members detect rather the negative $TNA \rightarrow PWC_u$ link, which is consistent
505 with the causal network from reanalysis (Fig. 5b). The thick line of the $TNA \rightarrow PWC_u$ connection in Fig. 7b suggests that
most of the CESM2 pacemaker simulations with nudged observed SSTAs in the equatorial Pacific simulate the opposite-sign
response from the Atlantic to the Pacific during the Atlantic-driven 1985-2014 regime before subtracting MEM. In the mean-
time, the positive-sign impact from the Pacific on the Atlantic (via either Niño3.4 or PWC on TNA) was detected by at least
two members in each experiment. For example, the $Ni\tilde{no}3.4 \rightarrow TNA$ link appears in the four experiments (all panels in Fig.
510 7). This link is more evident when MEM is subtracted during the second period as Fig. 7d shows more ensemble members
to simulate the link (thicker $Ni\tilde{no}3.4 \rightarrow TNA$ link) compared to Fig. 7b. The simulations from the pacemaker ensemble agree
greatly with the proposed contemporaneous negative PNA relationship to NAO (Honda et al., 2001). This was mostly detected
as contemporaneous $PNA \rightarrow NAO$ links in Fig. 7a-c and as $NAO \rightarrow PNA$ in Fig. 7d. As can be seen from Fig. 7, the similarities
with the causal networks from observational data (Fig. 5) entail an important role of ENSO (in combination with external



515 forcing) in shaping SST variability over the Atlantic. While the PNA-NAO connection is found positive and lagged in observa-
tions during the 1950-1983 period (Fig. 5a and c), it is detected as a negative contemporaneous connection in most pacemaker
simulations. Removing external forcing for the Pacific-driven 1950-1983 regime did not have a significant effect in the case of
reanalysis and the same for the pacemaker ensemble except for the vanishing $PWC_u \rightarrow TNA$ link. The relationship between
ENSO and PNA is, however, detected by fewer simulations when removing external forcing, and it is illustrated in Fig. 7c by
520 a thinner and weaker (on average) positive Niño3.4 \rightarrow PNA link compared to the one in Fig. 7a.

The importance of both ENSO and external forcing is further manifested during the 1985-2014 period through the emergence
of the negative sign effect from the Atlantic (TNA) on the Pacific (Niño3.4 through PWC), similar to the observations (Fig. 5b).
On the other hand, when subtracting MEM from the pacemaker simulations, more members show the positive Niño3.4 \rightarrow TNA
link (Fig. 7d) while the significant negative TNA \rightarrow PWC_u link is not detected (Fig. 7d vs. 7b). We recall that this is different
525 in the causal networks from the observed 1985-2014, which feature the negative TNA \rightarrow PWC_u before and after subtracting
the MEM (Fig. 5b and d). This apparent effect of external forcing being the main driver of an Atlantic-driven regime during
the second period is nevertheless implied by the results from the correlation/regression analysis in the previous section (Fig.
4d vs 3d) and the sensitivity test in Supplementary Fig. S1. Subtracting external forcing during the most recent period resulted
530 in a change in the direction of the link between PWC_u and Niño3.4 and the link between NAO and PNA. As the directions
of contemporaneous links were decided by majority rule (the most frequent direction of a particular lag-zero link among all
ensemble members during a specific run), Fig. 7d shows that more ensemble members detected those links in the opposite
direction (Niño3.4 \rightarrow PWC_u and NAO \rightarrow PNA).

The observed Niño3.4 time series in Fig. 6a is similar to the pacemaker ensemble mean (because SSTAs over the Niño region
are nudged towards observed values; small differences, most likely originating from observational uncertainty, ERSSTv5 vs
535 HadISST). The pacemaker ensemble mean TNA (red lines in Fig. 6b) implies an important role of ENSO in shaping SSTAs
over the Atlantic, possibly through combining internal variability processes and modulating the effects of external forcing.
Despite several discrepancies between the observed and the pacemaker-simulated TNA indices during the years following
major volcanic eruptions (e.g. the early 1990s) and during important El Niño / La Niña events (e.g. 1997–1998), the pacemaker
ensemble follows similar variations to the observed TNA through most of the 1950 to early 2000s period (red solid and dashed
540 lines compared to black lines). The fact that prescribing SSTAs only in the equatorial Pacific resulted in TNA SSTAs similar
to observations emphasizes the role of ENSO in the Atlantic-Pacific interactions and undermines the role of internal variability
in driving SST variability over the Atlantic during most of the analyzed period. Literature suggests that ENSO (Maher et al.,
2015, 2018) and its decadal imprint, PDV (Allen et al., 2014; Dong et al., 2014), have contributions from external drivers,
especially volcanic and anthropogenic aerosols. Other studies show that recent periods of global warming hiatus are the results
545 of anthropogenic aerosols modulating the phase of PDV rather than canceling out other warming effects (Kaufmann et al.,
2011; Smith et al., 2016). The results in Fig. 7 also suggest that the coupling between Atlantic and Pacific SSTs is moderately
strong in the CESM2 model during Niño events, explaining the appearance of Niño3.4 \rightarrow TNA (and/or $PWC_u \rightarrow$ TNA) links
in all causal networks on Fig. 7 (a-d). This also explains the large discrepancies between the pacemaker ensemble mean
(lines in red) and observations (lines in black) in Fig. 6b during significant El Niño years. The main difference between the



550 reanalysis and pacemaker causal networks remains during the Atlantic-driven regime after removing external forcing. Figure
6b shows increasing differences between the observed and the pacemaker-simulated TNA after the year 2000. This difference
might be due to the overestimation of the 1998-2013 global warming rate in CMIP6 climate models (McBride et al., 2021;
Smith et al., 2021; Fyfe et al., 2021; Smith and Forster, 2021; Tokarska et al., 2020a, b), and inherently in MEM. Different
factors contributing to such overestimation in CMIP6 have been proposed including the high equilibrium climate sensitivity
555 (ECS) that results in too strong warming responding to anthropogenic GHGs or too weak cooling responding to aerosols
(Intergovernmental Panel on Climate Change, 2013; Tokarska et al., 2020a; Schlund et al., 2020; Smith and Forster, 2021; Wei
et al., 2021). According to Wei et al. (2021), ECS only plays a partial role in the failure of most CMIP6 models in simulating the
early 2000s global warming slowdown. Instead, the authors attribute the discrepancy between observed and CMIP6-simulated
warming trends mostly to the models' deficiencies in simulating major modes of internal variability at interannual, interdecadal,
560 and multidecadal scales, thus excluding their potential effects (e.g. the cooling effect of PDV switching to a negative phase in
the early 2000s).

The different sources of external forcing, the overestimation of most recent warming trends, and the coincidence of volcanic
eruptions with ENSO events complicate the attribution of external contributions to the Atlantic-Pacific interactions during the
last decades of the historical record. To further test whether the observed teleconnections (including a change in the regime
565 of Atlantic-Pacific interactions) would arise only from internal climate variability, the next section presents results from a
pre-industrial control run of the CESM2 model.

4.3 Pre-industrial control simulations

Given 120 years of unforced simulation, we use the CESM2 pre-industrial run to analyze the causal connections between the
Atlantic and Pacific during their different states.

570 Figure 8a shows the long-term state of the two basins through the smoothed time series of AMV (solid; red and blue) and
PDV (dashed; pink and light blue) indices from 120 years of CESM2 pre-industrial control simulation. We define three 40-year
periods (160 seasons each) and we reconstruct a causal network for each that represents the connections between the Atlantic
and Pacific basins. We investigate such periods the same way we did for reanalysis data and the Pacific pacemaker simulations
in Sect. 4.1 and 4.2, respectively, focusing on the links between the Atlantic and Pacific modes. The causal graphs initially
575 displayed several links of different link strengths. Here in Fig. 8b, we show only the strongest links (with absolute value link
coefficients above the arbitrary threshold of 0.15; i.e. enhanced link colors).

The first 40-year period in Fig. 8a (P1) corresponds to PDV mainly in a positive phase while AMV is trending from a negative
to a neutral state. During this period Niño3.4 SST changes were found to strongly affect the PWC-associated zonal winds (1
season lagged positive Niño3.4 \rightarrow PWC_u link; P1 in Fig. 8b). These wind-induced changes are detected to affect extra-tropical
580 PNA mode with a 1-season lag (positive PWC_u \rightarrow PNA). The PNA changes are detected to be affected by NAO changes as
well (NAO \rightarrow PNA). The causal graph shows that the Pacific was contributing to tropical North Atlantic SSTA changes mainly
through the extra-tropical pathway, detected as a contemporaneous positive PNA \rightarrow TNA link, where the lower pressure center
at the southeastern lobe of the PNA pattern reduces the Atlantic northeasterlies, trapping warm water over the TNA region.



Pre-industrial Control

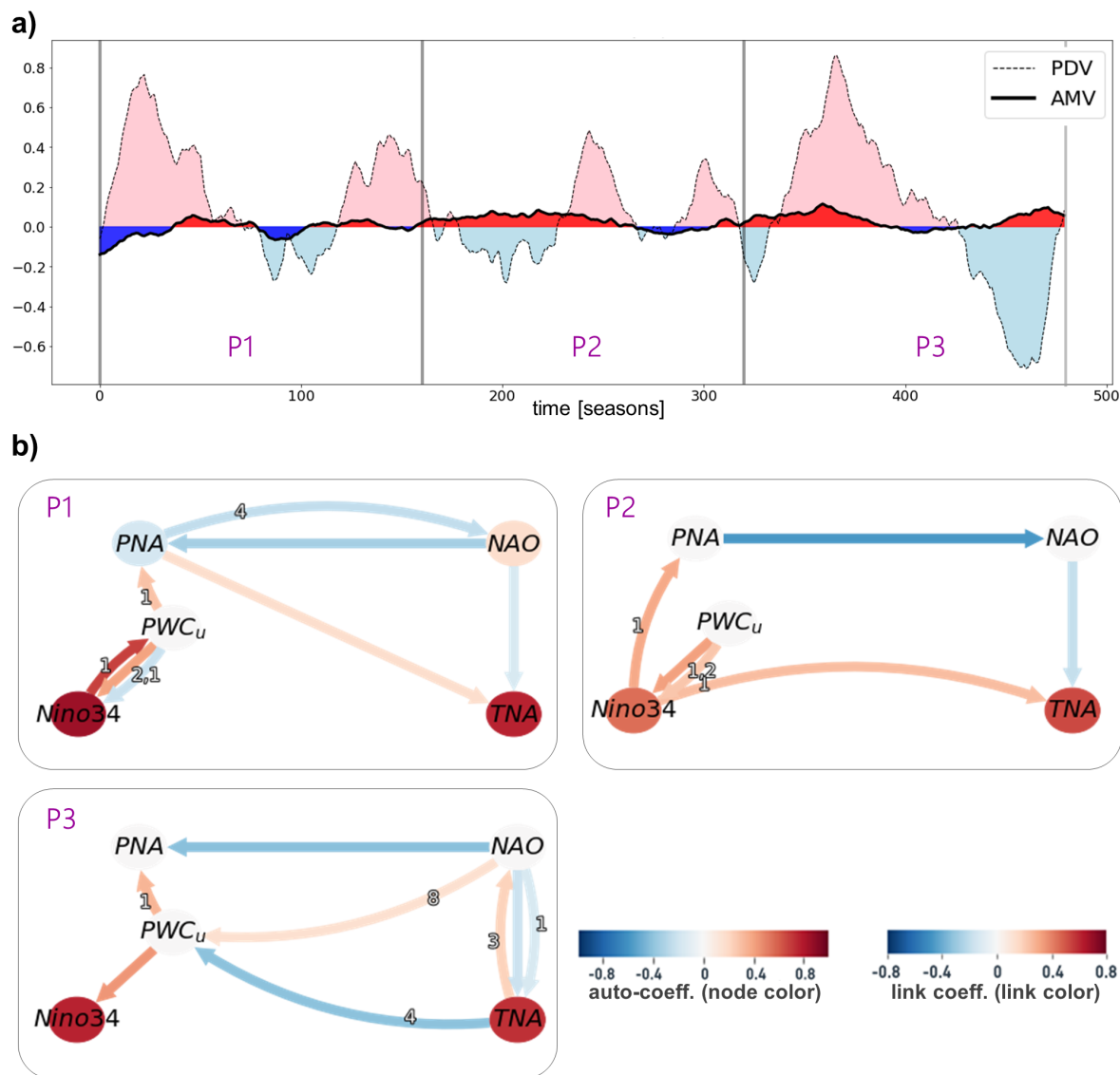


Figure 8. CESM2 pre-industrial control simulation. a) Smoothed AMV and PDV indices (10-year low-pass filtered) illustrating the decadal internal variability over the Atlantic and Pacific for 120 years (480 time steps [seasons]). We divide the time series into three 40-year periods (labelled P1, P2 and P3; 160 seasons each), which express different states of AMV and PDV. b) For every period (P1-3) selected in panel (a), we show the respective causal network, similar to reanalysis data (Fig. 5) and pacemaker simulations (Fig. 7).



The second period (P2 in Fig. 8a) illustrates a mostly positive AMV (trending negative towards the end of P2) while the PDV
585 switches from a negative to a positive phase. The causal graph (P2 in Fig. 8b) features a positive Niño3.4→PNA link and a
strong negative contemporaneous PNA→NAO link. The ENSO-induced changes are also found to contribute to the TNA SST
anomalies (positive Niño3.4→TNA link). Both tropical (Niño3.4→TNA) and extra-tropical (Niño3.4→PNA→NAO→TNA)
routes suggest the Pacific was mainly driving the Atlantic during this period.

The third period (P3 in Fig. 8a) shows PDV trending from a strong positive phase to a strong negative phase while the
590 AMV curve shows mainly positive SSTAs. The corresponding causal graph (P3 in Fig. 8b) shows that the warm TNA SSTAs
strongly contributed to La Niña conditions over the Pacific through strengthening the PWC (strong negative 4-season lagged
TNA→PWC_u link), cooling the Pacific on the decadal timescale (see PDV during P3 in Fig. 8a). The warming SST trends
in the Atlantic favor a strengthened PWC which ultimately cools the SSTs over the Niño3.4 due to enhanced upwelling. The
effect of the Atlantic on the Pacific during this period is manifested in the extra-tropics as well where NAO is found to strongly
595 contribute to PNA variability (contemporaneous NAO→PNA link).

The PNA→NAO connection is stronger in P2 compared to the NAO→PNA links in P1 and P3. The relatively weak
magnitudes of PDV anomalies during P2 (compared to P1 and P3; Fig. 8a) suggest reduced ENSO amplitude and hence
limited ENSO-like tropical forcing during that period (despite the lagged Niño3.4→PNA). The absence of strong El Niño
forcing might explain the strength of the PNA connection to NAO in P2, as suggested by Lin and Derome (2004); Soulard and
600 Lin (2017).

What can be concluded from the analysis of the pre-industrial run could be summarized as follows: (i) Pacific-driven and
Atlantic-driven regimes, and the phase switch between them, happen naturally in the absence of anthropogenic forcing. (ii)
This does not reject the possibility that human-induced forcing contributed greatly to at least the observed 1985-2014 changes.
(iii) The strength, direction, and lags of the cross-basins' seasonal-to-interannual interactions are modulated by the long-term
605 state of the two basins (PDV and AMV).

5 Discussion and Conclusions

Serving as a "proof of concept" within the domain of comprehending complex climate phenomena, the El Niño event of
1997/1998 presents a notable example showcasing the efficacy of causal discovery in discerning the underlying drivers that
govern well-established connections among contributing coupled processes (methods, Sect. 3.2.1). Hereupon, the scope extends
610 beyond ENSO, delving into the less-explored topic of Atlantic-Pacific interactions. Conventional regression and correlation
methods offered indications of a regime shift in the Atlantic-Pacific interactions during the observed historical 1950-2014
period (Meehl et al., 2021; Park et al., 2023). The correlation maps also showed that external forcing (represented by CMIP6
MEM) likely played a major role in setting the negative sign for the relationship between the TNA index and north tropical
Pacific SSTAs during the Atlantic-driven 1985-2014 period (Fig. 4d vs 3d). However, these approaches could not explore the
615 underlying pathways of these effects, which causal graphs provide by uncovering intricate causal relationships.



Based on causal graphs derived from reanalysis data and Pacific pacemaker simulations before separating the externally forced signal (a and b in Fig. 5 and 7), we find the Pacific's same sign influence on Atlantic during 1950-1983, aligning with prior reports (Meehl et al., 2021; Park et al., 2023). Estimated positive links from Niño3.4 (or PWC_u) to TNA represent the tropical pathway where El Niño and the modified Walker Circulation prompt equatorial Atlantic anticyclonic activity, weakening trade winds, and warming North Atlantic as a result of reduced evaporation. Other pathways recognized through PNA and NAO have also been detected. Positive causal links Niño3.4 (or PWC_u)→PNA and PNA→TNA highlight the extra-tropical path for the Pacific-induced effect on TNA. El Niño-associated Rossby wave propagation enhances Southeast United States low-pressure center (positive PNA phase), weakening North Atlantic trade winds and promoting TNA warming (Klein et al., 1999; García-Serrano et al., 2017; Jiang and Li, 2019). The transition from a Pacific-driven to an Atlantic-driven regime is evident in reanalysis and Pacific pacemaker simulations. During 1985-2014, causal graphs reveal lagged negative TNA→PWC links, denoting intensifying easterly trade winds affecting ENSO. Proposed mechanisms involve Rossby wave energy generated by enhanced precipitation over anomalously warm TNA region, impacting subtropical Pacific and causing easterly wind anomalies and La Niña-like cooling (Wang et al., 2017b; Park and Li, 2019; Park et al., 2022). Similar to reanalysis data, Pacific pacemaker simulations distinguish Pacific and Atlantic-driven regimes in SST responses (directly or via PWC). In the meantime, pacemaker-simulated SLP-based indices denote negative contemporaneous NAO-PNA relationship during 1950-1983 and 1985-2014. Notably, reanalysis identified positive 7-season lagged causal links during the first period, for which mechanisms are unclear.

The study involved separating external forcing from internal variability by subtracting CMIP6 MEM, yielding insights into external forcing's impact on Pacific-Atlantic interactions. Although MEM removal had modest effects on Pacific-driven regime causal graphs (panel c vs. a; Fig. 5 and 7), pronounced impacts emerged in the following period (panel b vs. d; Fig. 5 and 7), aligning with correlation and regression maps (Fig. 4d vs. 3d). During the Atlantic-driven era (1985-2014), reanalysis graphs highlighted TNA's strong contribution to same-season NAO changes (Fig. 5b), reversed after MEM subtraction (Fig. 5d). Additionally, a shift in the extra-tropical route linking the Pacific and Atlantic was observed during that period. Importantly, a negative TNA to ENSO response (via PWC) persisted despite MEM removal. In contrast, aggregated pacemaker graphs underscored external forcing's primary role in the Atlantic-driven regime, as evidenced by the vanishing TNA to PWC link and the emergence of Pacific-driven causal links after external forcing was removed. We note that the discrepancy between reanalysis and pacemaker aggregated causal graphs regarding the effect of subtracting MEM during 1985-2014 lessened when conducting a sensitivity test. Initiating the Atlantic-driven regime a year later (1986 instead of 1985) in the reanalysis yielded no detected negative TNA→PWC link after MEM removal (Supplementary Fig. S1), in line with correlation maps and aggregated pacemaker graphs for 1985-2014. A major role played by external forcing in the negative effect of TNA on ENSO falls in agreement with recent studies highlighting an increasing impact of external forcing on North Atlantic SSTAs and associated effects in recent decades (Murphy et al., 2017; Klavans et al., 2022; He et al., 2023). This brings additions to the debate over the attribution of the recently observed strengthening of the PWC, i.e. we suggest external forcing contributions modulated by the Atlantic might have amplified the recent PWC strengthening, in contrast with previous studies suggesting a dominant role of internal variability (Chung et al., 2019). Major disparities between observed and CESM2 pacemaker-simulated



TNA indices (during the Atlantic-driven period) were discussed in Sect. 4.2 and attributed to the extensively investigated post-2000s warming overestimation in CMIP6 (Tokarska et al., 2020b, a; Smith et al., 2021; Fyfe et al., 2021; Smith and Forster, 2021). The pacemaker-simulated TNA index (Fig. 6b) time series revealed a moderately strong coupling in the CESM2 model between Atlantic and Pacific SSTs, resulting in major differences in magnitude with the observed TNA following important El Niño events. This might explain the appearance of Niño3.4→TNA (and/or PWC_u→TNA) links in all aggregated causal networks in Fig. 7 (a-d).

The analysis of the historical record (1950-2014) suggests external forcing's potential contributions, yet doesn't exclude the role of internal variability driven by the Pacific and Atlantic long-term states (PDV and AMV). To explore Atlantic-Pacific internal variability interactions in unforced conditions, we utilized a 120-year CESM2 pre-industrial control run, divided into three 40-year periods. During two periods (P1 and P2), the causal graphs underscore the Pacific's impact on TNA variability through the tropical and extra-tropical pathways. Whereas for the third period (P3), characterized by a predominantly positive AMV and a significant PDV phase switch, a robust lagged negative TNA→PWC_u link was evident, similar to Atlantic-driven regime causal graphs in reanalysis (Fig. 5b and d) and pacemaker simulations with externally forced signal (Fig. 7b). The lag for the TNA effect on PWC differs between the pre-industrial control run (four seasons in P3) and observations/pacemaker ensemble (one season). In short, our pre-industrial control analysis indicates that both contrasting response regimes arise naturally without anthropogenic external forcing, influenced by the long-term states of the Pacific and Atlantic basins.

Throughout this study, causal discovery revealed varying signs and lags for the links between PNA and NAO. Earlier research proposed a robust negative correlation between Aleutian and Icelandic lows only during specific historical sub-periods (e.g., mid-1970s to mid-1990s; Honda et al., 2001; Pinto et al., 2011). This might clarify the absence of contemporaneous negative PNA→NAO links during the causal analysis for the Pacific-driven 1950-1983 era in reanalysis (Fig. 5a and c), where lagged positive connections were observed. However, prior studies haven't outlined mechanisms for such multi-season lagged positive associations. Conversely, the simultaneous negative PNA-NAO link was consistently identified across pacemaker and pre-industrial control runs. This link could be the result of Rossby wave-breaking events connecting PNA to opposite NAO phases (Song et al., 2009) or simply because, particularly in certain seasons, the two modes are spatially overlapping projections of the same variability pattern, connecting the Aleutian and Icelandic lows (Soulard and Lin, 2017).

In a concluding remark, the authors would like to highlight that causal discovery is a powerful tool to assess the physical mechanisms of Atlantic-Pacific interactions. However, a careful selection of the potential variables representing the analyzed mechanisms and the length of the time series are crucial for a robust application of causal analysis and reliable interpretation of detected connections. We experienced issues such that the algorithm rejected/added some connections when the analyzed period was prolonged or shortened and/or shifted by a few years. Therefore in order to make credible conclusions based on the application of causal discovery, it is important to accurately determine the causal assumptions, clarify the correct confounding variables, and analyze the interactions at their most relevant time scales to achieve robust results.

Finally, this study aims to enhance our understanding of the teleconnections between the Atlantic and Pacific oceans and their variability under different regimes. The findings emphasize the significance of external forcing, particularly in the most recent regime, and highlight the roles of ENSO, tropical and extra-tropical pathways, and internal variability in shaping SST



variability over the Atlantic on seasonal to interannual timescales. Further research is warranted to refine our knowledge of these complex interactions and improve model simulations to capture the observed teleconnections more accurately. External forcing represented by the CMIP6 MEM has contributions from natural (e.g. solar radiation, volcanic eruptions) and anthropogenic sources (e.g. aerosols, GHGs) with time and space-varying effects, hence, we encourage further analysis using simulations
690 with single external forcing sources (e.g. aerosol-only or GHG-only simulations) to increase the understanding and attribution of the observed changes in the climate system.

Code and data availability. The CESM2 Pacific pacemaker ensemble dataset can be found here: <https://www.earthsystemgrid.org/dataset/ucar.cgd.cesm2.pacific.pacemaker.html> [data set](last access: 07 August 2023). The Earth System Model Evaluation Tool (ESMValTool Righi et al., 2020) has been used for preprocessing and calculating the CMIP6 MEM. The Tigramite package for causal discovery is available
695 under the following public GitHub repository: <https://github.com/jakobrunge/tigramite/> [code] (last access: 07 August 2023, Runge et al. (2023)). The code used to produce the figures for this paper is accessible at the time of publication of the paper in the following GitHub repository: xxx, last access: xxxxxx, (Karmouche, 2023).

Author contributions. SF lead the study, the writing of the manuscript, and performed all the analysis. All co-authors contributed to the concept of the study, to the interpretation of the results, and to the writing of the manuscript

700 *Competing interests.* The authors declare no competing interests.

Acknowledgements. This study was funded by the European Research Council (ERC) Synergy Grant “Understanding and modeling the Earth System with Machine Learning (USMILE)” under the Horizon 2020 research and innovation programme (Grant agreement No. 855187). EG is supported by Central Research Development Fund at the University of Bremen, Funding No: ZF04A/2023/FB1/Galytska Evgenia. We acknowledge the World Climate Research Programme’s (WCRP’s) Working Group on Coupled Modelling (WGCM), and we thank the
705 CMIP-participating climate-modeling groups for producing and making available their model output. We also thank the CVCWG for publicly publishing their CESM2 pacemaker simulations. This work used resources of the Deutsches Klimarechenzentrum (DKRZ) granted by its Scientific Steering Committee (WLA) under project no. bd1083. We also acknowledge the use of AI tools for tasks including formatting, spell-checking, and the automated generation of references in the Bibtex format.



References

- 710 Allen, R. J., Norris, J. R., and Kovilakam, M.: Influence of anthropogenic aerosols and the Pacific Decadal Oscillation on tropical belt width, *Nature Geoscience*, 7, 270–274, 2014.
- Barnett, T. P.: Variations in near-global sea level pressure, *Journal of Atmospheric Sciences*, 42, 478–501, 1985.
- Bayr, T., Dommenges, D., Martin, T., and Power, S. B.: The eastward shift of the Walker circulation in response to global warming and its relationship to ENSO variability, *Clim. Dynam.*, 43, 2747–2763, 2014.
- 715 Bellucci, A., Mariotti, A., and Gualdi, S.: The role of forcings in the twentieth-century North Atlantic multidecadal variability: The 1940–75 North Atlantic cooling case study, *Journal of Climate*, 30, 7317–7337, 2017.
- Bjerknes, J.: A possible response of the atmospheric Hadley circulation to equatorial anomalies of ocean temperature, *Tellus*, 18, 820–829, 1966.
- Bjerknes, J.: Atmospheric teleconnections from the equatorial Pacific, *Monthly weather review*, 97, 163–172, 1969.
- 720 Booth, B. B., Dunstone, N. J., Halloran, P. R., Andrews, T., and Bellouin, N.: Aerosols implicated as a prime driver of twentieth-century North Atlantic climate variability, *Nature*, 484, 228–232, 2012.
- Borchert, L. F., Koul, V., Menary, M. B., Befort, D. J., Swingedouw, D., Sgubin, G., and Mignot, J.: Skillful decadal prediction of unforced southern European summer temperature variations, *Environ. Res. Lett.*, 16, 104 017, <https://doi.org/10.1088/1748-9326/ac20f5>, 2021.
- Brönnimann, S.: Impact of El Niño–Southern Oscillation on European climate, *Reviews of Geophysics*, 45, RG3003, 2007.
- 725 Brönnimann, S., Xoplaki, E., Casty, C., Pauling, A., and Luterbacher, J.: ENSO influence on Europe during the last centuries, *Climate Dynamics*, 28, 181–197, 2007.
- Capotondi, A., Deser, C., Phillips, A. S., Okumura, Y., and Larson, S. M.: ENSO and Pacific Decadal Variability in the Community Earth System Model Version 2, *Journal of Advances in Modeling Earth Systems*, 12, e2019MS002 022, <https://doi.org/https://doi.org/10.1029/2019MS002022>, e2019MS002022 2019MS002022, 2020.
- 730 Casselman, J. W., Taschetto, A. S., and Domeisen, D. I. V.: Nonlinearity in the Pathway of El Niño–Southern Oscillation to the Tropical North Atlantic, *Journal of Climate*, 2021.
- Cassou, C. and Terray, L.: Oceanic forcing of the wintertime low-frequency atmospheric variability in the North Atlantic European sector: A study with the ARPEGE model, *Journal of Climate*, 14, 4266–4291, 2001.
- Cassou, C., Cherchi, A., and Kosaka, Y., eds.: AR6, Annex IV: Modes of Variability, pp. 2153–2192, IPCC, Cambridge, United Kingdom and New York, NY, USA, 2021.
- 735 Chen, D., Zhang, X., Li, T., Wang, B., and Liang, X.: ENSO Dynamics in the E3SM-1-0, CESM2, and GFDL-CM4 Climate Models, *Journal of Climate*, 34, 10 193–10 213, 2021.
- Chung, E. S., Timmermann, A., Soden, B. J., and et al.: Reconciling opposing Walker circulation trends in observations and model projections, *Nat. Clim. Chang.*, 9, 405–412, <https://doi.org/10.1038/s41558-019-0446-4>, 2019.
- 740 Chylek, P., Folland, C., Klett, J. D., and Dubey, M. K.: CMIP5 climate models overestimate cooling by volcanic aerosols, *Geophys. Res. Lett.*, 47, e2020GL087 047, <https://doi.org/10.1029/2020GL087047>, 2020.
- Copernicus Climate Change Service, Climate Data Store: ORAS5 global ocean reanalysis monthly data from 1958 to present [data set], DOI: 10.24381/cds.67e8eeb7, accessed on 20-07-2023, 2021.
- Danabasoglu, G., Lamarque, J.-F., Bacmeister, J., Bailey, D. A., DuVivier, A. K., Edwards, J., Emmons, L. K., Fasullo, J., Garcia, R., Gettel-
- 745 man, A., Hannay, C., Holland, M. M., Large, W. G., Lauritzen, P. H., Lawrence, D. M., Lenaerts, J. T. M., Lindsay, K., Lipscomb, W. H.,



- Mills, M. J., Neale, R., Oleson, K. W., Otto-Bliesner, B., Phillips, A. S., Sacks, W., Tilmes, S., van Kampenhout, L., Vertenstein, M., Bertini, A., Dennis, J., Deser, C., Fischer, C., Fox-Kemper, B., Kay, J. E., Kinnison, D., Kushner, P. J., Larson, V. E., Long, M. C., Mickelson, S., Moore, J. K., Nienhouse, E., Polvani, L., Rasch, P. J., and Strand, W. G.: The Community Earth System Model Version 2 (CESM2) [data set], *Journal of Advances in Modeling Earth Systems*, 12, e2019MS001916, <https://doi.org/https://doi.org/10.1029/2019MS001916>, e2019MS001916 2019MS001916, 2020.
- 750 Deser, C.: Certain uncertainty: The role of internal climate variability in projections of regional climate change and risk management, *Earth's Future*, 8, e2020EF001854, 2020.
- Deser, C. and Phillips, A. S.: A range of outcomes: the combined effects of internal variability and anthropogenic forcing on regional climate trends over Europe, *Nonlinear Processes in Geophysics*, 30, 63–84, 2023.
- 755 Deser, C., Phillips, A., Bourdette, V., and Teng, H.: Uncertainty in climate change projections: the role of internal variability, *Climate dynamics*, 38, 527–546, 2012.
- Deser, C., Simpson, I. R., McKinnon, K. A., and Phillips, A. S.: ENSO and Pacific Decadal Variability in the Community Earth System Model Version 2 (CESM2), *Journal of Advances in Modeling Earth Systems*, 12, e2019MS002010, 2020.
- DiNezio, P. N., Vecchi, G. A., and Clement, A. C.: Detectability of changes in the Walker circulation in response to global warming, *J. Clim.*, 760 26, 4038–4048, 2013.
- Doblas-Reyes, F. J., García-Serrano, J., Cassou, C., Douville, H., and Giannini, A.: Revisiting the ENSO Teleconnection to the Tropical North Atlantic., *Journal of Climate*, 30, 2017.
- Dong, L. and McPhaden, M. J.: The role of external forcing and internal variability in regulating global mean surface temperatures on decadal timescales, *Environmental Research Letters*, 12, 034011, 2017.
- 765 Dong, L., Zhou, T., and Chen, X.: Changes of Pacific decadal variability in the twentieth century driven by internal variability, greenhouse gases, and aerosols, *Geophysical Research Letters*, 41, 8570–8577, 2014.
- Enfield, D. B. and Mayer, D. A.: Tropical Atlantic sea surface temperature variability and its relation to El Niño-Southern Oscillation, *Journal of Geophysical Research: Oceans*, 102, 929–945, 1997.
- Enfield, D. B., Mestas-Núñez, A. M., Mayer, D. A., and Cid-Serrano, L.: How ubiquitous is the dipole relationship in tropical Atlantic sea 770 surface temperatures?, *Journal of Geophysical Research: Oceans*, 104, 7841–7848, 1999.
- Eyring, V., Bony, S., Meehl, G. A., Senior, C. A., Stevens, B., Stouffer, R. J., and Taylor, K. E.: Overview of the Coupled Model Intercomparison Project Phase 6 (CMIP6) experimental design and organization, *Geosci. Model Dev.*, 9, 1937–1958, <https://doi.org/10.5194/gmd-9-1937-2016>, 2016.
- Eyring, V., Cox, P. M., Flato, G. M., Gleckler, P. J., Abramowitz, G., Caldwell, P., Collins, W. D., Gier, B. K., Hall, A. D., Hoffman, F. M., 775 Hurtt, G. C., Jahn, A., Jones, C. D., Klein, S. A., Krasting, J. P., Kwiatkowski, L., Lorenz, R., Maloney, E., Meehl, G. A., Pendergrass, A. G., Pincus, R., Ruane, A. C., Russell, J. L., Sanderson, B. M., Santer, B. D., Sherwood, S. C., Simpson, I. R., Stouffer, R. J., and Williamson, M. S.: Taking climate model evaluation to the next level, *Nat. Clim. Change*, 9, 102–110, <https://doi.org/10.1038/s41558-018-0355-y>, 2019.
- Eyring, V., Gillett, N. P., Achuta Rao, K. M., Barimalala, R., Barreiro Parrillo, M., Bellouin, N., Cassou, C., Durack, P. J., Kosaka, Y., 780 McGregor, S., Min, S.-K., Morgenstern, O., and Sun, Y.: *Human Influence on the Climate System*, pp. 423–552, Cambridge University Press, Cambridge, United Kingdom and New York, NY, USA, <https://doi.org/10.1017/9781009157896.005>, 2021.
- Fasullo, J. T., Phillips, A. S., and Deser, C.: Evaluation of leading modes of climate variability in the CMIP archives, *Journal of Climate*, 33, 5527–5545, 2020.



- Fyfe, J. C., Kharin, V. V., Santer, B. D., Cole, J. N. S., and Gillett, N. P.: Significant impact of forcing uncertainty in a large ensemble of
785 climate model simulations, *Proceedings of the National Academy of Sciences*, 118, <https://doi.org/10.1073/pnas.2016549118>, 2021.
- Galytska, E., Weigel, K., Handorf, D., and et al.: Causal model evaluation of Arctic-midlatitude teleconnections in CMIP6, *Authorea*,
<https://doi.org/10.1002/essoar.10512569.1>, 2022.
- García-Serrano, J., Cassou, C., Douville, H., Giannini, A., and Doblas-Reyes, F. J.: Revisiting the ENSO teleconnection to the tropical North
Atlantic, *Journal of Climate*, 30, 6945–6957, 2017.
- 790 Gerhardus, A. and Runge, J.: High-recall causal discovery for autocorrelated time series with latent confounders, *Advances in Neural Infor-*
mation Processing Systems, 33, 12 615–12 625, 2020.
- Gill, A. E.: Some simple solutions for heat-induced tropical circulation, *Quarterly Journal of the Royal Meteorological Society*, 106, 447–462,
1980.
- Ham, Y.-G., Kug, J.-S., Park, J.-Y., and Jin, F.-F.: Sea surface temperature in the north tropical Atlantic as a trigger for El Niño/Southern
795 Oscillation events, *Nature Geoscience*, 6, 112–116, 2013.
- Haustein, K., Otto, F. E. L., Venema, V., Jacobs, P., Cowtan, K., Hausfather, Z., Way, R. G., White, B., Subramanian, A., and Schurer, A. P.:
A limited role for unforced internal variability in twentieth-century warming, *Journal of Climate*, 32, 4893–4917, 2019.
- He, C., Clement, A., Kramer, S., et al.: Recent Atlantic multidecadal variability and its impacts are driven by external forcings, PREPRINT
(Version 1) available at Research Square, <https://doi.org/10.21203/rs.3.rs-2561784/v1>, 2023.
- 800 Hersbach, H., Bell, B., Berrisford, P., Biavati, G., Horányi, A., Muñoz Sabater, J., Nicolas, J., Peubey, C., Radu, R., Rozum, I., Schepers,
D., Simmons, A., Soci, C., Dee, D., and Thépaut, J.-N.: ERA5 monthly averaged data on single levels from 1940 to present, DOI:
10.24381/cds.f17050d7, accessed on 18-07-2023, 2023.
- Honda, M., Nakamura, H., Ukita, J., Kousaka, I., and Takeuchi, K.: Interannual seesaw between the Aleutian and Icelandic lows. Part I:
Seasonal dependence and life cycle, *Journal of Climate*, 14, 1029–1042, 2001.
- 805 Hurrell, J. W. and Deser, C.: North Atlantic climate variability: the role of the North Atlantic Oscillation, *Journal of marine systems*, 79,
231–244, 2010.
- Intergovernmental Panel on Climate Change: *Climate Change 2013: The Physical Science Basis. Contribution of Working Group I to the
Fifth Assessment Report of the Intergovernmental Panel on Climate Change*, Cambridge University Press, Cambridge, 2013.
- Jiang, L. and Li, T.: Relative roles of El Niño-induced extratropical and tropical forcing in generating Tropical North Atlantic (TNA) SST
810 anomaly, *Climate Dynamics*, 53, 3791–3804, 2019.
- Kalnay, E., M. K. R. K. W. C. D. D. L. G. M. I. S. S. G. W. J. W. Y. Z. M. C. W. E. W. H. J. J. K. M. C. R. J. W. A. L. R. R. R. J.
and Joseph, D.: The NCEP/NCAR 40-Year Reanalysis Project [data set], *Bulletin of the American Meteorological Society*, 77, 437–471,
[https://doi.org/10.1175/1520-0477\(1996\)077<0437:TNYRP>2.0.CO;2](https://doi.org/10.1175/1520-0477(1996)077<0437:TNYRP>2.0.CO;2), 1996.
- Karmouche, S., Galytska, E., Runge, J., Meehl, G. A., Phillips, A. S., Weigel, K., and Eyring, V.: Regime-oriented causal model evaluation
815 of Atlantic–Pacific teleconnections in CMIP6, *Earth System Dynamics*, 14, 309–344, 2023.
- Kaufmann, R. K., Kauppi, H., Mann, M. L., and Stock, J. H.: Reconciling anthropogenic climate change with observed temperature
1998–2008, *Proceedings of the National Academy of Sciences*, 108, 11 790–11 793, 2011.
- Klavans, J. M., Cane, M. A., Clement, A. C., and Murphy, L. N.: NAO predictability from external forcing in the late 20th century, *npj
Climate and Atmospheric Science*, 4, 1–9, 2021.
- 820 Klavans, J. M., Clement, A. C., Cane, M. A., and Murphy, L. N.: The Evolving Role of External Forcing in North Atlantic SST Variability
over the Last Millennium, *Journal of Climate*, 35, 2741–2758, 2022.



- Klein, S. A., Soden, B. J., and Lau, N.-C.: Remote sea surface temperature variations during ENSO: Evidence for a tropical atmospheric bridge, *Journal of climate*, 12, 917–932, 1999.
- Kociuba, G. and Power, S. B.: Inability of CMIP5 models to simulate recent strengthening of the Walker circulation: implications for
825 projections, *J. Clim.*, 28, 20–35, 2015.
- Kosaka, Y. and Xie, S.-P.: Recent global-warming hiatus tied to equatorial Pacific surface cooling, *Nature*, 501, 403–407, 2013.
- Kucharski, F., Kang, I.-S., Farneti, R., and Feudale, L.: Tropical Pacific response to 20th century Atlantic warming, *Geophysical Research Letters*, 38, 2011.
- Kucharski, F., Parvin, A., Wang, C., and Farneti, R.: Atlantic forcing of Pacific decadal variability, *Climate Dynamics*, 47, 433–449, 2016.
- 830 Kumar, A., Jha, B., and Wang, H.: Attribution of SST variability in global oceans and the role of ENSO, *Climate dynamics*, 43, 209–220, 2014.
- Latif, M. and Grötzner, A.: The equatorial Atlantic oscillation and its response to ENSO, *Climate Dynamics*, 16, 213–218, 2000.
- Lee, S.-K., Enfield, D. B., and Wang, C.: Why do some El Niños have no impact on tropical North Atlantic SST?, *Geophysical Research Letters*, 35, 2008.
- 835 Lengaigne, M., Boulanger, J.-P., Menkes, C., Madec, G., Delecluse, P., Guilyardi, E., and Slingo, J.: The March 1997 Westerly Wind Event and the Onset of the 1997/98 El Niño: Understanding the Role of the Atmospheric Response, *Journal of Climate*, 16, 3622–3638, 2003.
- Levine, A. F., McPhaden, M. J., and Frierson, D. M.: The impact of the AMO on multidecadal ENSO variability, *Geophysical Research Letters*, 44, 3877–3886, 2017.
- Li, X., Xie, S.-P., Gille, S. T., and Yoo, C.: Atlantic-induced pan-tropical climate change over the past three decades, *Nature Climate Change*,
840 6, 275–279, 2016.
- Lin, H. and Derome, J.: Nonlinearity of the extratropical response to tropical forcing, *Journal of climate*, 17, 2597–2608, 2004.
- Luo, J.-J., Sasaki, W., and Masumoto, Y.: Indian Ocean warming modulates Pacific climate change, *Proceedings of the National Academy of Sciences*, 109, 18 701–18 706, 2012.
- L’Heureux, M. L., Lee, S., and Lyon, B.: Recent multidecadal strengthening of the Walker circulation across the tropical Pacific, *Nature*
845 *Climate Change*, 3, 571–576, 2013.
- Maher, N., McGregor, S., England, M. H., and Gupta, A. S.: Effects of volcanism on tropical variability, *Geophysical Research Letters*, 42, 6024–6033, 2015.
- Maher, N., Matei, D., Milinski, S., and Marotzke, J.: ENSO change in climate projections: forced response or internal variability?, *Geophysical Research Letters*, 45, 11–390, 2018.
- 850 Mann, M. E., Steinman, B. A., and Miller, S. K.: On forced temperature changes, internal variability, and the AMO, *Geophysical Research Letters*, 41, 3211–3219, 2014.
- Mantua, N. J., Hare, S. R., Zhang, Y., Wallace, J. M., and Francis, R. C.: A Pacific interdecadal climate oscillation with impacts on salmon production, *Bulletin of the American Meteorological Society*, 78, 1069–1080, 1997.
- Matsuno, T.: Quasi-geostrophic motions in the equatorial area, *Journal of the Meteorological Society of Japan. Ser. II*, 44, 25–43, 1966.
- 855 McBride, L. A., Hope, A. P., Canty, T. P., Bennett, B. F., Tribett, W. R., and Salawitch, R. J.: Comparison of CMIP6 historical climate simulations and future projected warming to an empirical model of global climate, *Earth System Dynamics*, 12, 545–579, <https://doi.org/10.5194/esd-12-545-2021>, 2021.
- McGregor, S., Timmermann, A., Stuecker, M. F., England, M. H., Merrifield, M., Jin, F.-F., and Chikamoto, Y.: Recent Walker circulation strengthening and Pacific cooling amplified by Atlantic warming, *Nature Climate Change*, 4, 888–892, 2014.



- 860 McPhaden, M. J.: Genesis and evolution of the 1997–98 El Niño, *Science*, 283, 950–954, <https://doi.org/10.1126/science.283.5404.950>, 1999.
- Meehl, G. A., Hu, A., Arblaster, J. M., Fasullo, J., and Trenberth, K. E.: Externally forced and internally generated decadal climate variability associated with the Interdecadal Pacific Oscillation, *J. Clim.*, 26, 7298–7310, 2013.
- Meehl, G. A., Hu, A., Santer, B. D., and Xie, S.-P.: Contribution of the Interdecadal Pacific Oscillation to twentieth-century global surface temperature trends, *Nature Climate Change*, 6, 1005–1008, 2016.
- 865 Meehl, G. A., Chung, C. T. Y., Arblaster, J. M., Holland, M. M., and Bitz, C. M.: Tropical Decadal Variability and the Rate of Arctic Sea Ice Decrease, *Geophysical Research Letters*, 45, 11,310–11,318, <https://doi.org/10.1029/2018GL079989>, 2018.
- Meehl, G. A., Hu, A., Castruccio, F., England, M. H., Bates, S. C., Danabasoglu, G., McGregor, S., Arblaster, J. M., Xie, S.-P., and Rosenbloom, N.: Atlantic and Pacific tropics connected by mutually interactive decadal-timescale processes, *Nature Geoscience*, 14, 36–42, 2021.
- 870 Menary, M. B., Robson, J., Allan, R. P., Booth, B. B. B., Cassou, C., Gastineau, G., and et al.: Aerosol-forced AMOC changes in CMIP6 historical simulations, *Geophysical Research Letters*, 47, e2020GL088166, <https://doi.org/10.1029/2020GL088166>, 2020.
- Milinski, S., Maher, N., and Olonscheck, D.: How large does a large ensemble need to be?, 2019.
- Murphy, L. N., Bellomo, K., Cane, M., and Clement, A.: The role of historical forcings in simulating the observed Atlantic multidecadal oscillation, *Geophysical Research Letters*, 44, 1847–1853, <https://doi.org/10.1002/2016GL071337>, 2017.
- 875 Neelin, J. D., Battisti, D. S., Hirst, A. C., Jin, F.-F., Wakata, Y., Yamagata, T., and Zebiak, S. E.: ENSO theory, *Journal of Geophysical Research: Oceans*, 103, 14 261–14 290, 1998.
- Newman, M., Alexander, M. A., Ault, T. R., Cobb, K. M., Deser, C., Di Lorenzo, E., Mantua, N. J., Miller, A. J., Minobe, S., Nakamura, H., Schneider, N., Vimont, D. J., Phillips, A. S., Scott, J. D., and Smith, C. A.: The Pacific decadal oscillation, revisited, *J. Climate*, 29, 4399–4427, <https://doi.org/10.1175/JCLI-D-15-0508.1>, 2016.
- 880 O’Brien, J. P. and Deser, C.: Quantifying and understanding forced changes to unforced modes of atmospheric circulation variability over the North Pacific in a coupled model large ensemble, *Journal of Climate*, 36, 19–37, 2023.
- Park, J.-H. and Li, T.: Interdecadal modulation of El Niño–tropical North Atlantic teleconnection by the Atlantic multi-decadal oscillation, *Climate Dynamics*, 52, 5345–5360, 2019.
- Park, J.-H., Li, T., Yeh, S.-W., and Kim, H.: Effect of recent Atlantic warming in strengthening Atlantic–Pacific teleconnection on interannual timescale via enhanced connection with the Pacific meridional mode, *Climate dynamics*, 53, 371–387, 2019.
- 885 Park, J.-H., Kug, J.-S., Yang, Y.-M., Oh, H., Zhao, J., and Wu, Y.: Role of the Climatological North Pacific High in the North Tropical Atlantic–ENSO Connection, *Journal of Climate*, 35, 3215–3226, 2022.
- Park, J.-H., Yeh, S.-W., Kug, J.-S., Yang, Y.-M., Jo, H.-S., Kim, H.-J., and An, S.-I.: Two regimes of inter-basin interactions between the Atlantic and Pacific Oceans on interannual timescales, *npj Climate and Atmospheric Science*, 6, 13, 2023.
- 890 Phillips, A. S., Deser, C., Fasullo, J., Schneider, D., and Simpson, I.: Assessing Climate Variability and Change in Model Large Ensembles: A User’s Guide to the “Climate Variability Diagnostics Package for Large Ensembles”, version 1, version, 1, 0, 2020.
- Pinto, J. G., Reyers, M., and Ulbrich, U.: The variable link between PNA and NAO in observations and in multi-century CGCM simulations, *Climate Dynamics*, 36, 337–354, 2011.
- Polyakov, I. V. and Johnson, M. A.: Arctic decadal and interdecadal variability, *Geophysical Research Letters*, 27, 4097–4100, 895 <https://doi.org/10.1029/2000GL011909>, 2000.
- Power, S. B. and Kociuba, G.: What caused the observed twentieth-century weakening of the Walker circulation?, *J. Clim.*, 24, 6501–6514, 2011.



- Rayner, N., Parker, D. E., Horton, E., Folland, C. K., Alexander, L. V., Rowell, D., Kent, E. C., and Kaplan, A.: Global analyses of sea surface temperature, sea ice, and night marine air temperature since the late nineteenth century, *Journal of Geophysical Research: Atmospheres*, 108, 2003.
- Righi, M., Andela, B., Eyring, V., Lauer, A., Predoi, V., Schlund, M., Vegas-Regidor, J., Bock, L., Brötz, B., de Mora, L., Diblen, F., Dreyer, L., Drost, N., Earnshaw, P., Hassler, B., Koldunov, N., Little, B., Loosveldt Tomas, S., and Zimmermann, K.: Earth System Model Evaluation Tool (ESMValTool) v2.0 – technical overview, *Geoscientific Model Development*, 13, 1179–1199, <https://doi.org/10.5194/gmd-13-1179-2020>, 2020.
- Runge, J.: Discovering contemporaneous and lagged causal relations in autocorrelated nonlinear time series datasets, in: *Conference on Uncertainty in Artificial Intelligence*, pp. 1388–1397, PMLR, 2020.
- Runge, J., Petoukhov, V., Donges, J. F., Hlinka, J., Jajcay, N., Vejmelka, M., Hartman, D., Marwan, N., Paluš, M., and Kurths, J.: Identifying causal gateways and mediators in complex spatio-temporal systems, *Nature communications*, 6, 8502, 2015.
- Runge, J., Nowack, P., Kretschmer, M., Flaxman, S., and Sejdinovic, D.: Detecting and quantifying causal associations in large nonlinear time series datasets, *Science advances*, 5, eaau4996, 2019.
- Runge, J., Gerhardus, A., Varando, G., Eyring, V., and Camps-Valls, G.: Causal inference for time series, *Nature Reviews Earth & Environment*, 10, 2553, <https://doi.org/http://dx.doi.org/10.1038/s43017-023-00431-y>, 2023.
- Ruprich-Robert, Y., Msadek, R., Castruccio, F., Yeager, S., Delworth, T., and Danabasoglu, G.: Assessing the climate impacts of the observed Atlantic multidecadal variability using the GFDL CM2. 1 and NCAR CESM1 global coupled models, *Journal of Climate*, 30, 2785–2810, 2017.
- Sato, Y., Goto, D., Michibata, T., Suzuki, K., Takemura, T., Tomita, H., and Nakajima, T.: Aerosol effects on cloud water amounts were successfully simulated by a global cloud-system resolving model, *Nat. Commun.*, 9, 985, <https://doi.org/10.1038/s41467-018-03379-6>, 2018.
- Scaife, A. A. and et al.: Skillful long-range prediction of European and North American winters, *Geophysical Research Letters*, 41, 2514–2519, 2014.
- Schlund, M., Lauer, A., Gentine, P., Sherwood, S. C., and Eyring, V.: Emergent constraints on equilibrium climate sensitivity in CMIP5: do they hold for CMIP6?, *Earth System Dynamics*, 11, 1233–1258, <https://doi.org/10.5194/esd-11-1233-2020>, 2020.
- Smith, C. J. and Forster, P. M.: Suppressed Late-20th Century Warming in CMIP6 Models Explained by Forcing and Feedbacks, *Geophysical Research Letters*, 48, e2021GL094948, <https://doi.org/https://doi.org/10.1029/2021GL094948>, e2021GL094948 2021GL094948, 2021.
- Smith, C. J., Harris, G. R., Palmer, M. D., Bellouin, N., Collins, W., Myhre, G., Schulz, M., Golaz, J.-C., Ringer, M., Storelvmo, T., et al.: Energy budget constraints on the time history of aerosol forcing and climate sensitivity, *Journal of Geophysical Research: Atmospheres*, 126, e2020JD033622, 2021.
- Smith, D., Booth, B., Dunstone, N., and et al.: Role of volcanic and anthropogenic aerosols in the recent global surface warming slowdown, *Nature Climate Change*, 6, 936–940, <https://doi.org/10.1038/nclimate3058>, 2016.
- Smith, D. M., Eade, R., Scaife, A. A., Caron, L.-P., Danabasoglu, G., DelSole, T. M., Delworth, T., Doblas-Reyes, F. J., Dunstone, N. J., Hermanson, L., Kharin, V., Kimoto, M., Merryfield, W. J., Mochizuki, T., Müller, W. A., Pohlmann, H., Yeager, S., and Yang, X.: Robust skill of decadal climate predictions, *npj Climate and Atmospheric Science*, 2, 13, <https://doi.org/10.1038/s41612-019-0084-4>, 2019.
- Smith, D. M., Gillett, N. P., Simpson, I. R., Athanasiadis, P. J., Baehr, J., Bethke, I., Bilge, T. A., Bonnet, R., Boucher, O., Findell, K. L., Gastineau, G., Gualdi, S., Hermanson, L., Leung, L. R., Mignot, J., Müller, W. A., Osprey, S., Otterå, O. H., Persad, G. G., Scaife, A. A., Schmidt, G. A., Shiogama, H., Sutton, R. T., Swingedouw, D., Yang, S., Zhou, T., and Ziehn, T.: Attribution of multi-annual to decadal



- changes in the climate system: The Large Ensemble Single Forcing Model Intercomparison Project (LESFMIP), *Frontiers in Climate*, 4, <https://doi.org/10.3389/fclim.2022.955414>, 2022.
- Song, J., Li, C., Zhou, W., and Pan, J.: The linkage between the Pacific-North American teleconnection pattern and the North Atlantic Oscillation, *Advances in Atmospheric Sciences*, 26, 229–239, 2009.
- 940 Soulard, N. and Lin, H.: The spring relationship between the Pacific-North American pattern and the North Atlantic Oscillation, *Climate Dynamics*, 48, 619–629, <https://doi.org/10.1007/s00382-016-3098-3>, 2017.
- Tebaldi, C., Dorheim, K., Wehner, M., and Leung, R.: Extreme Metrics and Large Ensembles, *Earth System Dynamics Discussions*, 2021, 1–59, 2021.
- Tokarska, K. B., Hegerl, G. C., Schurer, A. P., Forster, P. M., and Marvel, K.: Observational constraints on the effective climate sensitivity
945 from the historical period, *Environmental Research Letters*, 15, 034043, <https://doi.org/10.1088/1748-9326/ab738f>, 2020a.
- Tokarska, K. B., Stolpe, M. B., Sippel, S., Fischer, E. M., Smith, C. J., Lehner, F., and Knutti, R.: Past warming trend constrains future warming in CMIP6 models, *Science Advances*, 6, eaaz9549, <https://doi.org/10.1126/sciadv.aaz9549>, 2020b.
- Trenberth, K. E.: The definition of El Niño, *Bulletin of the American Meteorological Society*, 78, 2771–2778, 1997.
- Trenberth, K. E. and Shea, D. J.: Atlantic hurricanes and natural variability in 2005, *Geophysical research letters*, 33, 2006.
- 950 Vecchi, G. A. and Soden, B. J.: Global warming and the weakening of the tropical circulation, *J. Clim.*, 20, 4316–4340, 2007.
- Wallace, J. M. and Gutzler, D. S.: Teleconnections in the geopotential height field during the Northern Hemisphere winter, *Monthly Weather Review*, 109, 784–812, 1981.
- Wang, C.: A review of ENSO theories, *National Science Review*, 5, 813–825, <https://doi.org/10.1093/nsr/nwy104>, 2018.
- Wang, J., Yang, B., Ljungqvist, F. C., Luterbacher, J., Osborn, T. J., Briffa, K. R., and Zorita, E.: Internal and external forcing of multidecadal
955 Atlantic climate variability over the past 1,200 years, *Nat. Geosci.*, 10, 512–517, <https://doi.org/10.1038/ngeo2962>, 2017a.
- Wang, L., Yu, J.-Y., and Paek, H.: Enhanced biennial variability in the Pacific due to Atlantic capacitor effect, *Nature Communications*, 8, 14887, 2017b.
- Watanabe, M. and Tatebe, H.: Reconciling roles of sulphate aerosol forcing and internal variability in Atlantic multidecadal climate changes, *Climate Dynamics*, 53, 4651–4665, 2019.
- 960 Wei, M., Shu, Q., Song, Z., Song, Y., Yang, X., Guo, Y., Li, X., and Qiao, F.: Could CMIP6 climate models reproduce the early-2000s global warming slowdown?, *Science China Earth Sciences*, 64, 853–865, <https://doi.org/10.1007/s11430-020-9740-3>, 2021.
- Wu, M., Zhou, T., Li, C., Li, H., Chen, X., Wu, B., Zhang, W., and Zhang, L.: A very likely weakening of Pacific Walker Circulation in constrained near-future projections, *Nature communications*, 12, 6502, 2021.
- Yang, Y.-M., An, S.-I., Wang, B., and Park, J. H.: A global-scale multidecadal variability driven by Atlantic multidecadal oscillation, *National
965 Science Review*, 7, 1190–1197, 2020.
- Zhang, R., Sutton, R., Danabasoglu, G., Kwon, Y.-O., Marsh, R., Yeager, S. G., Amrhein, D. E., and Little, C. M.: A review of the role of the Atlantic Meridional Overturning Circulation in Atlantic Multidecadal Variability and associated climate impacts, *Rev. Geophys.*, 57, 316–375, <https://doi.org/10.1029/2019RG000644>, 2019.
- Zhao, X. and Allen, R. J.: Strengthening of the Walker Circulation in recent decades and the role of natural sea surface temperature variability,
970 *Environmental Research Communications*, 1, 021003, 2019.